AN ABSTRACT OF THE THESIS OF

Walter Frederick Burns for the degree of Master of Science

in Chemistry presented on March 16, 1978

Title: SLOW PROCESSES IN GAS-SOLID CHROMATOGRAPHY

Abstract approved: Redacted for Privacy

Stephen J. Hawkes

Gas-solid chromatography often has asymmetrical elution peaks. This is attributed to nonlinear isotherms, multi-energy adsorption sites, and slow processes. This study utilized a stop-flow gas chromatograph with various NaOH and NaCl modified aluminas as adsorbents and methane as adsorbate to determine the influence of surface area and pore volume distribution on the slow process rate constant. It was found that Knudsen diffusion from micropores was the cause of the slow process for this system.

# Slow Processes in Gas-Solid Chromatography

by

Walter Frederick Burns

A THESIS

submitted to

Oregon State University

in partial fulfillment of
the requirements for the
degree of

Master of Science

Completed March 1978

Commencement June 1978

Approved

Redacted for Privacy

Professor of Chemistry
in charge of major

Redacted for Privacy

Chairman of Department of Chemistry

Redacted for Privacy

Dean of Graduate School

Date thesis is presented March 16, 1978

Typed by Opal Grossnicklaus for Walter Frederick Burns

TABLE OF CONTENTS

LIST OF FIGURES

# LIST OF TABLES

# SLOW PROCESSES IN GAS-SOLID CHROMATOGRAPHY

## I. INTRODUCTION

The principle of partitioning impurities onto adsorbent surfaces in the purification of gases and liquids has been practiced for many years. Gas-solid chromatography (GSC) was first practiced by Eucken and Knick (1) in 1936 and was further developed by petroleum chemists in the 1940's (2). It was not popular as a separation technique and was largely neglected after gas-liquid chromatography (GLC) was introduced (3) in 1952. Recently, however, many applications have been found where GSC is superior to GLC (4, 5) and has come into its time along with GLC as an important chromatographic technique. Gas-solid columns have a number of advantages over gas-liquid columns in that the surfaces are stable over wide temperature ranges, there is no problem with column bleed and often the selectivity for certain types of compounds is much greater in GSC than GLC.

The neglect of GSC arose from a number of causes, the most important of which was the asymmetry and broadness of the eluting peaks. These are often attributed to nonlinear adsorption isotherms (6), surface heterogeneity (7) and slow processes (8). Other problems in GSC results from the large surface areas and high adsorbent-adsorbate interaction energies. Increased operating temperatures

of 50-75° are often necessary for comparable elution times with GLC columns. The increased temperature and sometimes catalytic nature of the surface may cause the sample to decompose. Thus most gas-solid columns have a more restricted range of application than do gas-liquid columns.

Methods have been described to reduce peak asymmetry by modifying the surface with water vapor (9), monolayers of organic phase (10, 11), or solid salts (7, 12, 13). The exact nature and the effect these have on the adsorption phenomenon and the adsorbent surfaces is not yet established. It has been shown by Phillips and Scott (7) that the original adsorbent surface area decreases somewhat, and the activity is changed considerably. They also found that log of surface area decreased in a linear relation to the weight percent coverage of NaOH, but not linearly with NaCl, NaBr or NaI. Scott (13) found that the retention volume of n-pentane on NaOH modified alumina decreased until 10 mole % where it leveled off. The polarity of the surface, as measured by the retention ratio of butadiene to n-pentane, reached a minimum at 10 mole % NaOH and then increased again. Sawyer et al. (14, 15) showed that retention volumes changed considerably for various solutes on various adsorbents and salt modifications. Several authors (7, 13, 16) have noted that the peak symmetry is improved with surface modification and have postulated that the original adsorbent surface has been covered with one or more

molecular layers of modifier so the most active sites are covered, or some of the pores plugged.

It is important in the future development of GSC adsorbents to determine whether the slow processes causing tails arise from slow diffusion from pores, or slow desorption from the most active sites. These slow processes may be studied by a quantitative comparison of a GSC and GLC analysis of identical samples, by comparison of GSC runs at different flow rates and temperatures, and by observing the slow bleed off after the main sample has been eluted from a GSC column, but most simply by the use of the stopped-flow technique. In this, a sample is injected onto the adsorbent column and the flow stopped for a few minutes at some point during the passage of the sample through the column. After restarting the flow the bulk of the sample is then eluted as a normal sharp peak. However, if the flow is stopped again for a few minutes, restarting the flow produces a chromatogram with a sharp peak of the sample at a retention time which depends predictably upon the point in the column where the main bulk of the sample was held in the original stop. Such a "memory" peak may be produced a number of times from one original injection. With only one stop, quantities of n-hexane have been slowly adsorbed and later slowly recovered in the range of 1 to 40% of the original sample (17).

Katsanos and Hadzistelios (18) utilized the stopped-flow

technique described by Phillips to determine the rate constants of the slow processes on alumina modified with Cerium (III) chloride. They found that for each adsorbate and temperature there were two distinct rate constants, presumably from two different energy sites. The activation energies calculated for the desorption of trans-2-butene were 4.5 Kcal/mole for the fastest and 11 Kcal/mole for the "slow" process.

This thesis discusses in detail the effects of slow desorption and slow transport mechanisms from adsorbent pores on chromatographic zone broadening and describes experiments similar to those of Phillips (17) and Katsanos (18) with a stopped-flow chromatographic system using salt modified adsorbent surfaces. The surface area and pore diameter changes of the surfaces are measured, the successive memory peak areas monitored, the rate constants calculated, and the results used to draw conclusions about the most probable mechanism of the slow process.

# II. THEORY

## A. Chromatographic Process

The two processes of central importance in gas chromatography are the partition of solute molecules in the stationary phase and the migration of solute in the carrier and stationary phase. The former describes a column's ability to distinguish between two compounds and is the selectivity. The selectivity can be varied by changing the stationary phase. The latter is also important in separating compounds and minimizing analysis time. By carefully controlling the length of solute migration, the zones of solute can be kept narrow, giving better separations. Zone spreading is expressed as plate height and is defined (19) as $\sigma^2/L$ and is equated to the sum of several terms

$$H = \frac{1}{1/A_c + 1/C_c V} + \frac{B}{V} + C_k V + C_m V \qquad \text{Eq. 1}$$

where H is the height equivalent to a theoretical plate; $A_c$ is the multipath or anastomosis term and accounts for the different lengths of the various streamlines of the carrier going down the column length; $C_c$ is the resistance to diffusion of the solute in the carrier gas perpendicular to the carrier flow; V is carrier gas velocity; B is the diffusion of solute molecules parallel to the column flow; $C_k$ describes the resistance to mass transfer from adsorption and desorption kinetics

on solid surfaces and $C_m$ is the resistance to mass transfer for solute molecules in the carrier near the surface and within the adsorbent particle.

Each of these terms contributes to the overall band broadening, but in this discussion the $C_k$ and $C_m$ terms are of special interest since these involve the multi-energy adsorption sites, and pore structure, respectively.

## B. Multi-energy Adsorption Sites

There are several reasons for variation in adsorption energy of the surface from place to place. First, impurities in the surface will cause a localized change in adsorption energies due to the different bonding and chemical potential of the impurity. Second, and more important since the development of synthetic high purity adsorbents, is surface roughness of the adsorbent. A site in a valley or pore will have a higher energy than one on the level. This can be seen by the Kelvin equation

$$\ln\frac{P}{P_0} = \frac{-2\gamma V \cos\theta}{RTr_k} \qquad \text{Eq. 2}$$

where $P_0$ is atmospheric pressure and $P/P_0$ is the relative pressure (in atm) at which pores of radius $r_k$ begin filling, $\gamma$ is the surface tension of the adsorbate with molar volume V, $\theta$ is the contact angle between adsorbate and adsorbent, and R and T are the gas constant

and temperature in Kelvin respectively.

From equation 2 it should be noted that the smallest pores fill first as $P/P_0$ increases. It has been postulated (20) that some of the smallest pores are filled long before a monolayer covers the surface. Even the most homogeneous surfaces known, i.e., graphitized carbon blacks, have variations in adsorption energies from this phenomenon.

Multi-energy adsorption sites and surface heterogeneity cause nonlinear isotherms and peak asymmetry with increasing sample size. The isotherms of adsorbents commonly used in GSC are convex with increasing sample size and coverage of the surface. This indicates the first adsorbed solute molecules find the highest energy adsorption sites while the remainder take the lower energy sites. In GSC the highest energy sites are filled first and emptied last and may require considerable time to desorb after the main peak profile has passed. This slow desorption phenomenon can be considered either as a kinetic or equilibrium effect.

The kinetic consideration assumes adsorption is rapid on all sites, but desorption is much slower on the higher energy sites due to the increased activation energy necessary to desorb the solute molecule from the surface. This is expressed by the Arrhenius equation

$$k = Ae^{(-W/RT)} \qquad \text{Eq. 3}$$

where K is the rate constant of the desorption process, A is the frequency factor of solute molecules hitting the surface and is about $10^{13}$/ sec, W is the activation energy of the process. R and T are the gas constant and temperature, respectively.

The equilibrium consideration says that the partition of solute between adsorbent and carrier gas for each site is dependent upon the adsorption energy as expressed by the Gibb's free energy expression for the desorption process.

$$\Delta G^\circ = -RT \ln K_{eq} \qquad \text{Eq. 4}$$

$$\text{and } K_{eq} = e^{(-\Delta G^\circ/RT)} \qquad \text{Eq. 5}$$

$$\text{where } K_{eq} = \frac{\text{moles solute in mobile phase}}{\text{moles solute on adsorbent}} \qquad \text{Eq. 6}$$

and $G^\circ$ is the standard Gibbs free energy; R and T are the gas constant and temperature in Kelvin respectively; $K_{eq}$ is the equilibrium constant.

As the solute concentration zone approaches, the highest energy sites become saturated first, long before the other sites are filled and remain saturated until the major portion of the zone has passed. Thus the tail is formed, because the higher energy sites have a smaller equilibrium constant and are not close to equilibrium as described by Gidding's nonequilibrium theory (21). As the zone moves through the column the tail becomes longer and longer and the high energy sites continually move farther out of equilibrium

with the mobile phase solute zone.

Giddings (22) has shown that if the energy difference between two types of sites $\Delta E_{21}$ = 10 Kcal/mole, the plate height contribution relative to uniform surfaces will be increased one million fold. For uniform surfaces the $C_k V$ term of equation 1 is found to be negligible and will remain so as long as the energy spread stays within the following bounds

$$\Delta E_{21} < 0.03\ T \qquad \text{Eq. 7}$$

where $\Delta E_{21}$ is the energy difference between the high and low energy site, and T is the Kelvin temperature.

For adsorption on multisite surfaces, the plate height contribution of the $C_k$ term is given by

$$C_k = 2\ R(1-R)\ \bar{t}_d \qquad \text{Eq. 8}$$

where R is the fraction of solute in the mobile phase at equilibrium and $\bar{t}_d$ is the mean desorption time of the solute.

## C. Surface Pore Structure

Pore structure is as important to adsorbent behavior as surface area and surface type. Wicke (23) examining charcoal and silica gel found that only 0.9 to 1.5 $m^2$/gm surface exists in macropores of 1000 Å, or larger, while 350-1700 $m^2$/gm surface exists in micropores less than 1000 Å. This indicates that the surface area

available for adsorption in macropores is negligible in comparison to the surface area in the micropores. Thus it is imperative to study the effects of pore structures and sizes and the mechanisms of solute transport into and out of the pores as this may be the rate limiting step of the adsorption process.

Bulk diffusion, following Fick's laws, is found in areas and pores where the distance between surfaces is greater than the molecular mean free path, and a molecule is more likely to collide with another molecule than the surface. Knudsen diffusion is the prominent gas phase transport mechanism in capillaries less than the molecular mean free path, about 1000 Å. Knudsen diffusion is much slower than bulk diffusion because most of the molecular collisions are with the capillary walls. The molecules may remain adsorbed there an average time $\tau$, then reevaporate without preference to direction. Knudsen diffusion along with adsorption on the capillary surface is given by

$$D_p = \frac{2d^2\bar{u}}{6(d+\bar{u}\tau)} \qquad \text{Eq. 9}$$

where $D_p$ is the diffusion coefficient, d the capillary diameter, $\bar{u}$ is the mean molecular velocity, and $\tau$ is the average sorption time. When $\tau = 0$ (no adsorption), equation 9 becomes

$$D_p = \frac{d\bar{u}}{3} \qquad \text{Eq. 10}$$

Differences in rates of Knudsen diffusion in comparable capillary diameters can arise from various pore structures. Long straight single capillaries will have a larger diffusion coefficient than capillaries with frequent and random changes in direction, so the possibility of long molecular flights without striking a surface is much reduced. Hiby and Pahl (24) found by tubes repeatedly bent at short intervals of length that the Knudsen diffusion coefficient changed remarkably as seen in Table I, below.

Table I. Effect of kinked capillaries on Knudsen diffusion constant.

| l/r | 2 | 3 | 4 | 5 | 10 |
|---|---|---|---|---|---|
| Dl/D∞ | 0.672 | 0.766 | 0.820 | 0.855 | 0.925 |

where l denotes the length of each straight section in the kinked tube of radius r, and Dl/D∞ is the diffusion coefficient ratio of the kinked tube to the straight capillary.

The third transport mechanism is surface flow. The molecules move from site to site along the surface, but never become completely separated from the surface until a corner or crevice is encountered. Generally this transport process is quite slow with rates similar to diffusion in liquids as the average distance the molecule can move on the sufrace is one molecular diameter. Liquid diffusion constants are about $10^{-5}$ as fast as gas diffusion constants. Even

though the surface transport mechanism may be slower than gas phase transport, the amount of material subject to each mechanism is proportional to the concentration in each phase. Hence, a strongly adsorbed molecule will have far greater surface transport out of a pore than by Knudsen diffusion, especially, since capillaries have higher adsorption energies because of the curved surface, and the molecules are most likely to be hitting the capillary surface. A weakly adsorbed molecule such as helium or methane will most likely be transported via Knudsen diffusion.

Clausing (25) showed that in most systems, the diffusion out of the pores is due mainly to surface migration. For example, $C_2H_5Cl$ at 60°C adsorbing on charcoal with capillaries of length $l = 0.1$ mm and diameter of 100 Å, the average sorbed time $\tau = 10^{-7}$ sec, the average velocity $\bar{u} = 3 \times 10^{4}$ cm/sec will have an average residence time of $2 \times 10^{-3}$ sec. In the absence of surface migration the molecules would have taken 2.5 sec to pass from the capillary by Knudsen diffusion.

The average residence time t for a molecule in a capillary is given by

$$t = \frac{l^2}{6D_p} \qquad \text{Eq. 11}$$

where t is the average residence time of a molecule in a pore, l is the capillary length, and $D_p$ is the diffusion coefficient from the pore.

The diffusion coefficient for a molecule which undergoes Knudsen diffusion, adsorption, and surface migration is given by (25)

$$D_p = \frac{2d^2\bar{u} + 3\tau L_m(\bar{u})^2}{6(d+\bar{u}\tau)} \qquad \text{Eq. 12}$$

where $L_m$ is the mean free path of the molecule on the surface.

In pores of small diameter, surface migration and adsorption become very important in the transport of sample from the pores as shown in Figure 1. A $\tau$ of $10^{-10}$ sec represents only weak to moderate adsorption, and often $\tau$ can be much longer as in the previous example where $\tau = 10^{-7}$ sec. As $\tau$ goes to zero the curve straightens, and becomes pure Knudsen diffusion at $\tau = 0$.

Kammermeyer and Rutz (26) plotted the permeability coefficient K for a series of gases against boiling, or critical temperature for gases flowing through Vycor porous glass. The plot should be such that at any one temperature, if gas phase mass transport is much greater than surface transport, $K\sqrt{m}$ should be constant for the series, where K is the permeability coefficient of the glass, m is the molecular weight of the gas in question. However, this is far from true as seen in Figure 2. $K\sqrt{m}$ increases smoothly with increasing condensibility of the flowing gases, so that significant surface transport must be occurring for gases of higher boiling point. It can be seen that

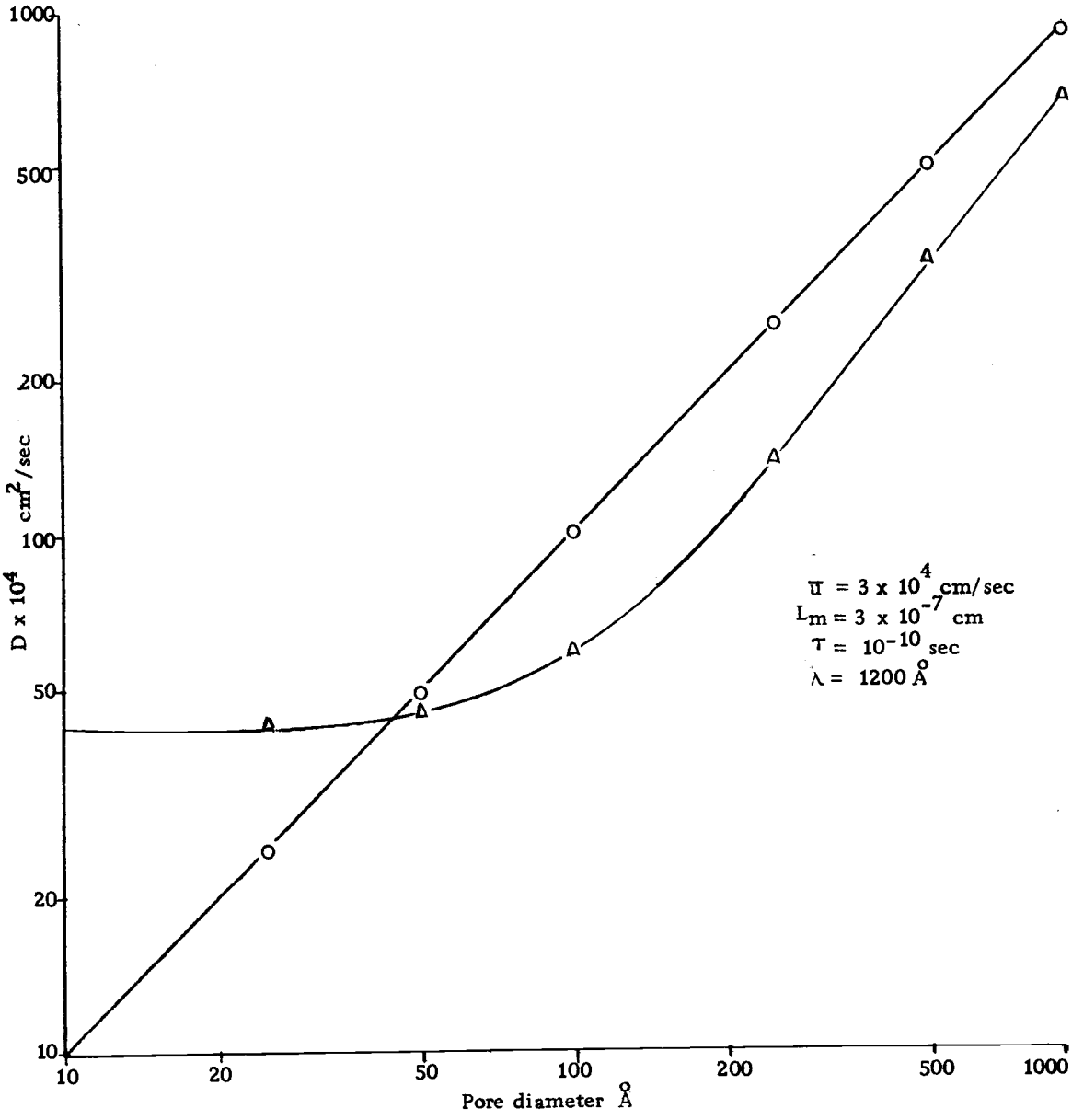


Figure 1. Diffusion coefficients from pores with Knudsen diffusion only (o); with Knudsen diffusion adsorption, and surface migration ( Δ ). Bulk diffusion coefficient is 0.21 $cm^2$/sec.

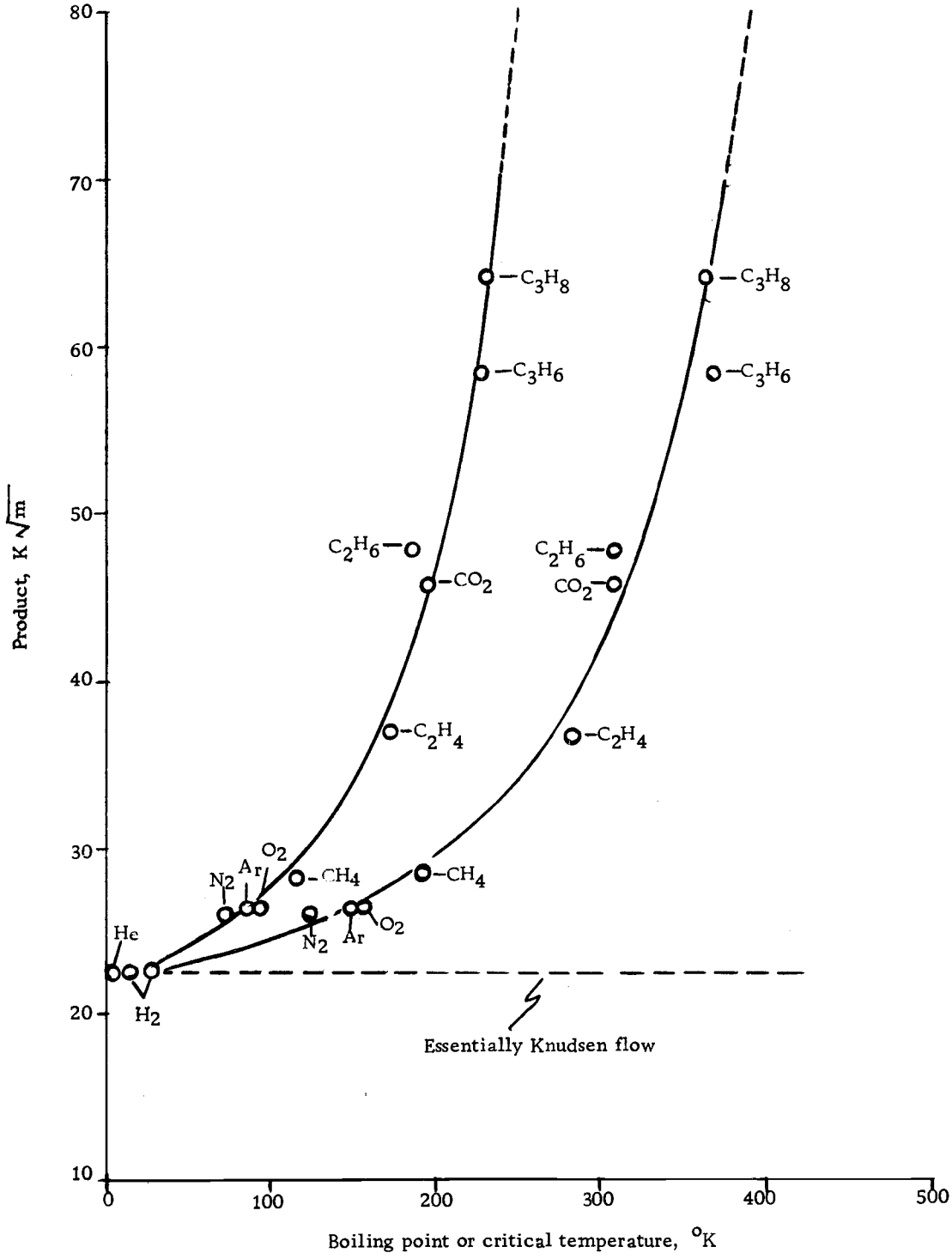


Figure 2. K $\sqrt{m}$ at 25°C plotted against boiling point $T_b$ and critical temperature $T_c$ for gases and vapors diffusing through Vycor porous glass (26).

surface migration of molecules larger than propane exceeds gas phase transport. Methane and helium have almost all of their transport via Knudsen diffusion, as they spend almost no time on the surface.

The contribution of the mobile phase mass transfer ($C_m$) within the adsorbent particles to the plate height is given by Giddings (27)

$$C_m = \frac{2(1-\emptyset R)^2 d_p^2}{60(1-\emptyset)\,\gamma_p D_p} \qquad \text{Eq. 13}$$

where $\emptyset$ is the fraction of mobile phase in interparticle space, R is the fraction of solute in the mobile phase at equilibrium, $d_p$ is the particle diameter, $\gamma_p$ the obstruction factor for diffusion within the particle, and $D_p$ is the diffusion coefficient from the pore.

In comparing this to non-porous material where the $C_m$ is given by

$$C_m = \frac{W d_p^2}{D_m} \qquad \text{Eq. 14}$$

where W is a dimensionless constant, and $D_m$ is diffusion in the bulk mobile phase.

It can be seen that the most important factor in equation 13 is $D_p^{-1}$. The $\emptyset R$ term is usually small so $(1-\emptyset R)^2$ is near unity. For comparison of the plate height contribution from porous adsorbents

described by equation 13 and the more or less ideal case described in equation 14 some typical values may be: $D_m = 0.2$, $d_p^2 = 1$, $W = 0.5$, $\phi = 0.25$, $R = 0.1$, $\gamma_p = 0.7$, $D_p = 2 \times 10^{-3}$. $C_m$ from equation 13 is 64 as opposed to 0.5 from 14; a $10^2$ increase. $D_m$ (bulk diffusion coefficient) was estimated (28) from

$$D_m = 0.599\,\lambda\,\bar{u} \qquad \text{Eq. 15}$$

where $\lambda$ is the mean free molecular path length about 1200 Å, and $\bar{u}$ is the average molecular velocity estimated at $3 \times 10^4$ cm/sec. $D_p$ was estimated from equation 10 with the pore diameter d = 20 Å.

## D. Rate Constant of the Slow Process

The theoretical section of this thesis has thus far shown that diffusion from small pores and/or desorption from multi-energy adsorption sites can play a major role in chromatographic peak broadening. The processes as described and occurring independently of each other, are simple one molecule interactions, and should follow first order kinetics. Assuming first order kinetics, and that the reaction is slow so that equilibrium is not reached, as does Katsanos (18), the rate constant k is defined as

$$k = -1/t \ln \frac{(a_0 - x_m)}{a_0} \qquad \text{Eq. 16}$$

where t is the time the reaction has progressed, $a_0$ is the initial mass of the sample adsorbed onto, or trapped in the adsorbent particle, and

$x_m$ is the mass of sample leaving the adsorbent particle over the period t. Then

$$a_0 - x = a_1 \qquad \text{Eq. 17}$$

where $a_1$ is the mass of sample remaining in the adsorbent at the end of flow period $t_1$ and at the beginning of the first stop flow period $t_1'$. Substituting equation 17 into 16, rearranging, and taking the anti-logarithm of both sides

$$a_1 = a_0 e^{-kt_1} \qquad \text{Eq. 18}$$

The first stop-flow period also loses sample from the absorbent particle described by equation 16. The initial amount at the beginning of the stop-flow period $t_1'$ was not $a_0$, but rather $a_1$.

$$kt_1' = -\ln \frac{(a_1 - x)}{(a_1)} \qquad \text{Eq. 19}$$

Substituting for $a_1$ from equation 18 into 19 and rearranging

$$x = a_0 e^{-kt_1} [1 - e^{-kt_1'}] \qquad \text{Eq. 20}$$

and taking the logarithm of both sides

$$\ln x + kt_1 = \ln [a_0(1 - e^{-kt_1'})] \qquad \text{Eq. 21}$$

The right side of equation 21 is a constant as long as the stop flow periods t' are constant for all subsequent stops. This is known

as Guggenheim's method (29), and for the $n^{th}$ stop-flow period

$$\ln x_n = k(t_1 + t_1' + t_2 + t_2' \ldots + t_n) + \ln [a_0(1-e^{-kt_n'})] \qquad \text{Eq. 22}$$

where $x_n$ is the mass of sample desorbed during the $n^{th}$ stop-flow period, $t_1$, $t_2$ .... $t_n$ are the periods when carrier gas is sweeping over the column and $t_1'$, $t_2'$ .... $t_n'$ are the periods the carrier gas is stopped in the column. When ln sample mass versus total time excluding the last stop-flow period, is plotted, a straight line of slope k should be obtained. If the line is curved and the slope not constant, there may be two reactions proceeding at different rates, i.e. the material may be in equilibrium with the fast adsorption sites, or the reaction may not be first order, and the initial assumption made was invalid.

# III. EXPERIMENTAL

## A. Preparation and Modification of Surfaces

The adsorbents used for this study were activated alumina H-151 (Analabs) 40-50 mesh. Before use they were acid washed in dilute (6 N) HCl as recommended by Sawyer et al. (14), to remove any iron that might be present as a contaminant on the surface. To insure the HCl reached into the inner surface of the adsorbent particle, the flask was evacuated by a Sargent-Welch vacuum pump until the HCl stopped frothing and bubbling. When the vacuum was released the HCl was driven into the pores by air pressure. After a few minutes the HCl was decanted off the alumina, followed by several distilled water rinses. The alumina was then washed into a sintered glass crucible and air was drawn over it until the adsorbent particles flowed freely. The alumina was then heated for 24 hours at 350°C to drive off the excess water.

The modification of the surfaces was done by weighing 10 gm of dry acid washed adsorbent and adding a calculated amount of reagent grade salt to distilled water and diluting to 100 ml. Fifty ml were then added to the adsorbent and the flask evacuated with the Sargent-Welch vacuum pump until the frothing and bubbling of the salt solution ceased (10 to 15 min). The vacuum was then released and the alumina washed into a coarse porosity sintered glass crucible using

the other 50 ml of salt solution. Air was drawn over the modified alumina until the particles flowed freely. The modified alumina was then heated to 350°C for at least 24 hours. The exact surface coverage was calculated from the total salt solution used during the modification procedure. Generally, it was found that 10 gm of the alumina could utilize 6-8 ml of solution. The percent modification was calculated from the following

$$\frac{(\text{gm salt}/100\text{ ml}) \times (\text{ml soln used})}{\text{gm adsorbent}} \times 100$$

$$= \%\ \text{Modification} \qquad \text{Eq. 23}$$

To obtain different percentage modifications the grams of salt dissolved in 100 ml $H_2O$ was varied.

B. Measurement of Surface Areas and Pore Diameters

The surface areas and pore diameters were obtained from Dr. Slabaugh's surface area apparatus (30) shown in Figure 3. The samples were heated to 350°C for several hours to drive off any adsorbed water and cooled in a desiccator. The samples were weighed into tiny buckets specially constructed from tin foil for this purpose. The buckets of adsorbent were then hung on the quartz springs of the instrument, the system closed and then evacuated for 24 hours. The chambers containing the samples (7 samples) were

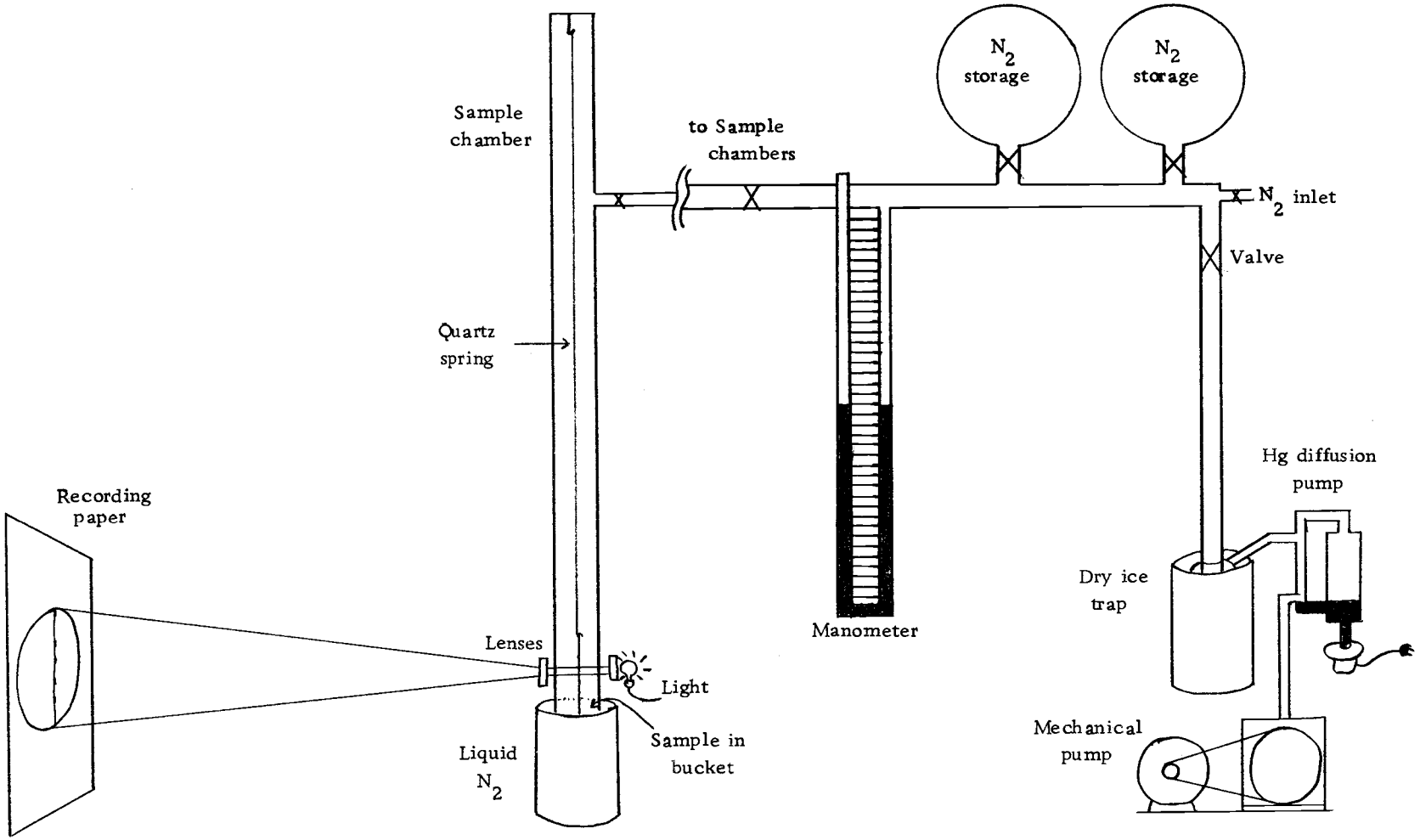


Figure 3. Surface area apparatus. Shows one of seven sample chambers.

immersed in liquid nitrogen, readings of partial pressure ($P/P_0$) and bucket height were then taken. A small amount of nitrogen was injected into the system; equilibrium was reached in about 15 minutes and the next readings of $P/P_0$ and bucket height were taken. This was continued until there were four to eight readings between $P/P_0 = 0$ and 0.2. Enough points were obtained to adequately determine the point B on the BET curve for the adsorbent. Point B is the point where the adsorbate forms a monolayer on the surface and the resulting isotherm straightens as shown in Figure 4.

For each point it is necessary to take both the equilibrium pressure reading and the distance the quartz springs moved. From this distance and knowing the particular spring constant the increase in weight is determined by

$$\Delta gm = dK_s/S \qquad \text{Eq. 24}$$

where $\Delta$ gm is the increase in weight/gm adsorbent, d is the distance the spring stretched, $K_s$ is the spring constant in mg/cm, and S is the sample weight. Each of these are then plotted as mg of $N_2$/gm adsorbent versus partial pressure of the nitrogen. Point B is determined by laying a straight edge on the level portion of the curve and choosing a point where the curve significantly left the straight edge. In most cases it was between $P/P_0 = 0.03$ to 0.04. The surface area in $m^2$/gm is then determined by

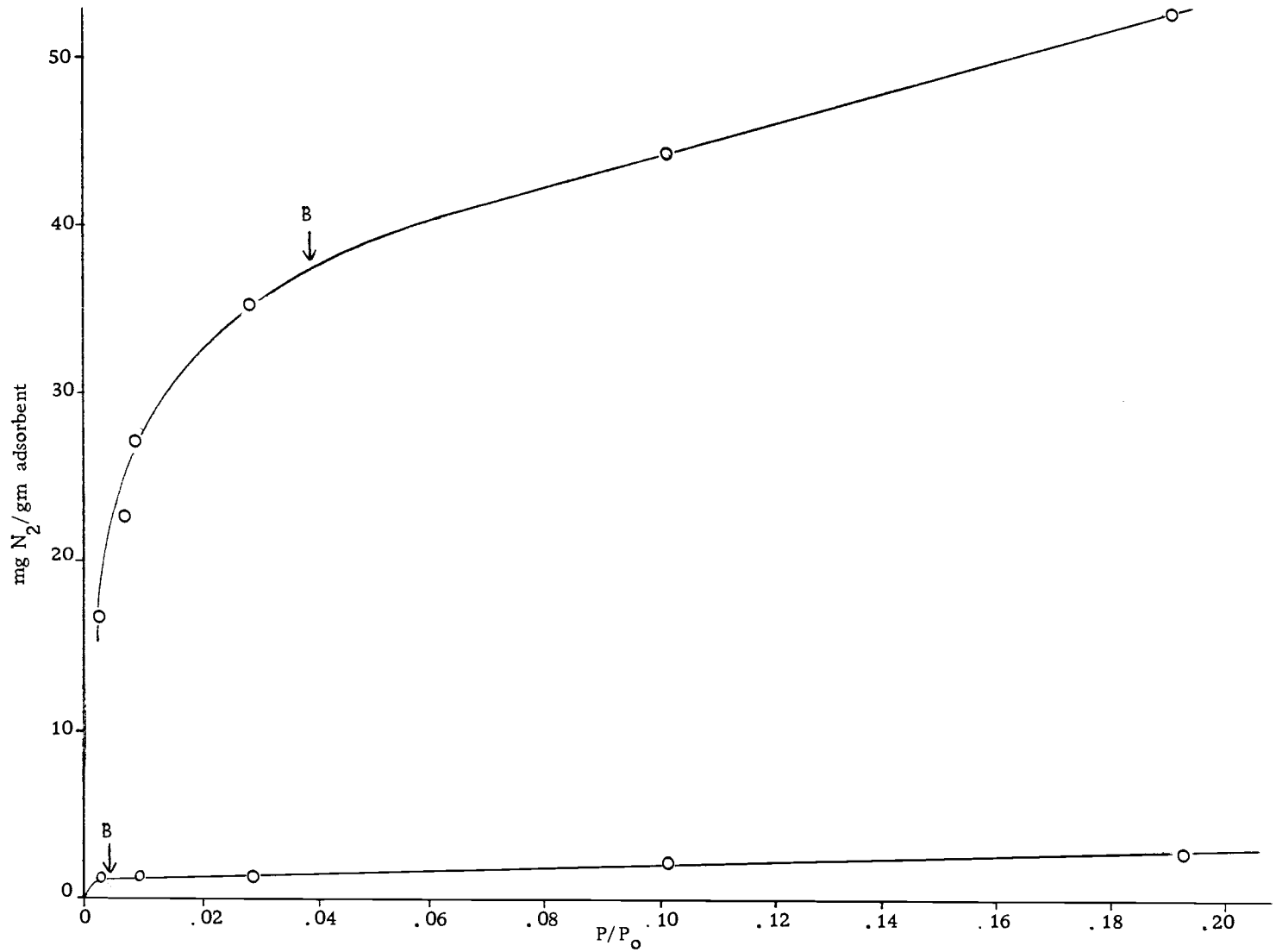


Figure 4. Point B on the isotherms of two adsorbents; one of large surface area and one of low surface area.

$$SA = \frac{(B)(N)(A)(10^{-20}\ m^2/\mathring{A}^2)(10^{-3}\ g/mg)}{M} \qquad \text{Eq. 25}$$

where SA is the surface area of the adsorbent in $m^2/gm$, B is the mg $N_2$/gm at point B on the curve, N is Avogadro's number, A is the area a single $N_2$ occupies on the surface and is assumed to be 16.4 $\mathring{A}^2$, M is the gm molecular weight of $N_2$. When the constants are calculated equation 25 becomes

$$SA = (B) \times (3.483) \qquad \text{Eq. 26}$$

The pore volumes and pore radii were determined by the hysteresis of the desorption leg of the isotherm. Hysteresis is the deviation of the desorption leg from the adsorption leg. This is shown in Figure 5. The adsorption isotherm was extended to $P/P_0$ = 0.95 by methods previously described. The desorption leg was produced successively by evacuating the chamber, allowing at least 15 minutes for equilibrium, and recording the $P/P_0$ and the distance the spring moved. Eight to ten points are necessary between $P/P_0$ = 0.95 and 0.20. Again using equation 24 the (mg $N_2$)/(gm adsorbent) versus $P/P_0$ on the desorption leg, one can calculate the weight of adsorbed $N_2$ in each average pore radius. The method of calculation is described by Pierce (31) and is found in Appendix I. When the pore volumes versus pore radii are plotted, the resulting histograms show the size pores containing the respective volumes.

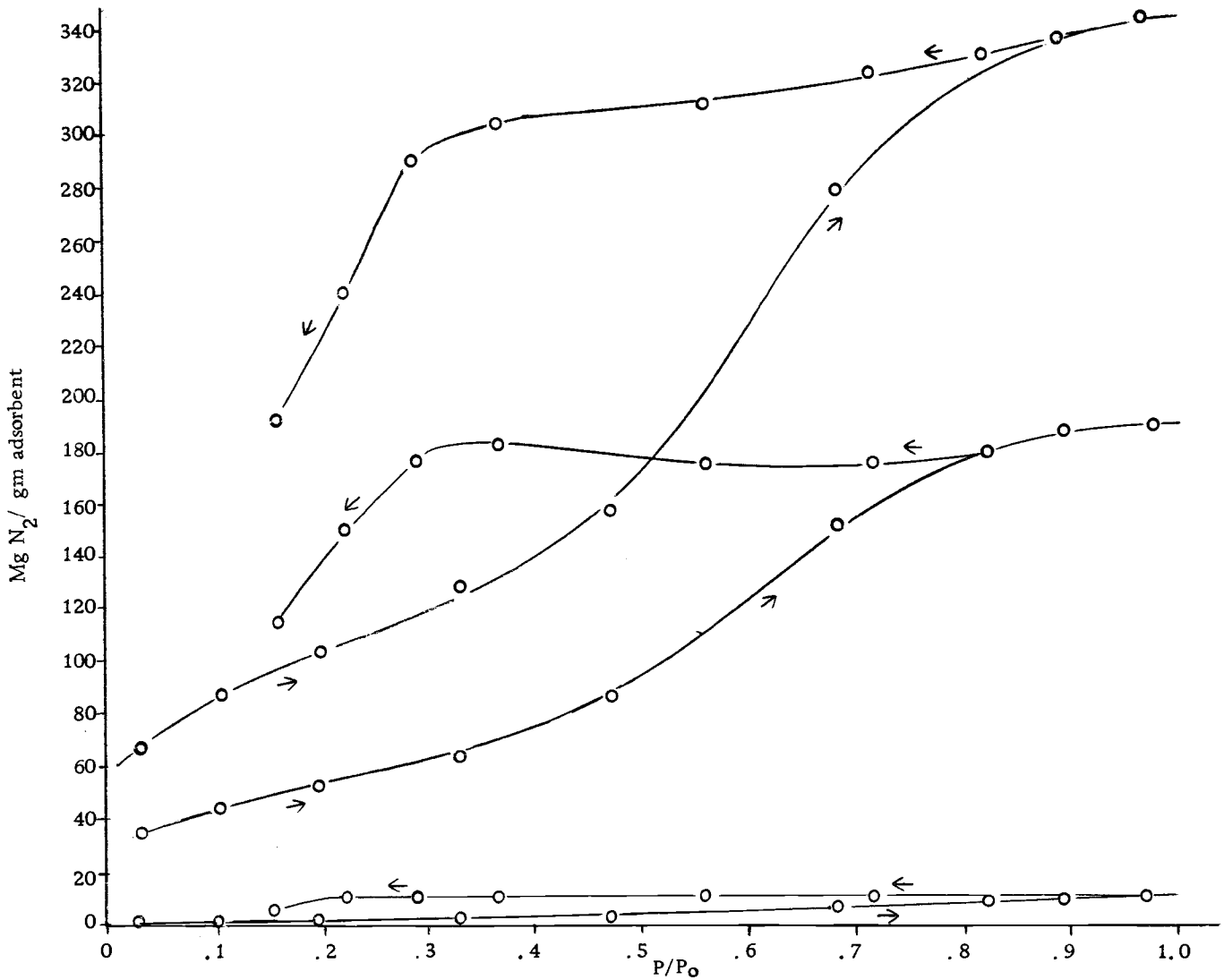


Figure 5. Desorption isotherm historesis for 3 samples of varying surface area. Arrows indicate direction of analysis.

## C. Measurement of the Slow Processes

The instrument used for measurement of the slow processes was a modified Perkin Elmer F-11 Gas Chromatograph with a Carle micro-thermal conductivity detector shown in Figure 6. The oven maintained the set temperatures to ±2°C. Two Loenco 6-port Linear 0-ring switch valves were used. The first and closest to the detector was the stopped flow/bypass valve. Its purpose was to stop the flow of the helium carrier in the column, while still allowing a bypass flow over the heated sensors of the detector. The second valve was the inject/elute valve. Its purpose was to divert the carrier gas flow and inject the standard methane over the adsorbent for the desired length of time. When the injection time was completed the valve was moved to the elute position where it remained until another injection. Only the column was placed in the oven. The high temperatures needed to activate the adsorbent could not be tolerated by the 0-ring valves or the detector, and since only methane was used, with no problems with condensation in the lines, these were maintained at room temperature. The detector is much more sensitive at low temperatures than high temperatures. The column was a 7' x 1/8" OD 316 stainless steel tube, with 40-50 mesh glass beads packed on both ends of the adsorbent slug. The column was packed by forcing the packing through the column by 50 psi air pressure, while tapping

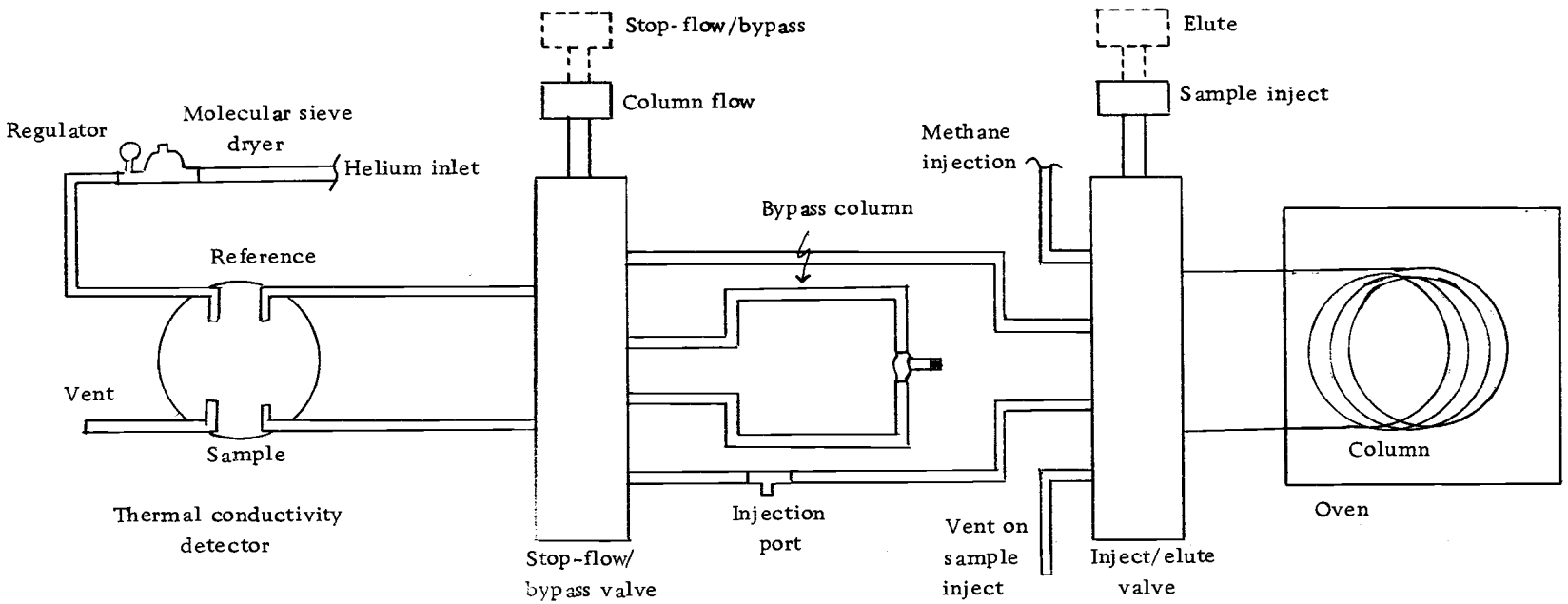


Figure 6. Stopped flow instrument to measure slow processes on adsorbent column.

gently. It was packed in three stages: glass beads, adsorbent, and finally, glass beads. The column ends were plugged with glass wool and the column was placed in the oven and heated to 320°C for several hours with helium passing over it. To this point the column outlet was not attached to the instrument to prevent desorbed water from condensing in the detector. The column was then connected, the detector current set at 25 mA, the column temperature adjusted to 200°C and the experiment begun.

The methane sample was injected onto the column by moving the inject/elute valve to the inject mode. The pure methane at 5 psi was then allowed to pass over the adsorbent for the desired time, 500 or 1000 seconds. The inject/elute valve was then moved to the elute position and the entire column was swept with helium at 7.5 ml/min for 60 seconds. The stopped flow/bypass valve was then moved into bypass position and the flow stopped over the column for 120 seconds. The column was then swept with carrier gas by moving the stopped flow/bypass valve into elute position and the memory peaks monitored. The carrier flow through the column was repetitively stopped for 120 seconds, each stop followed by a 60 second elution until the memory peaks were no longer measurable. The output profile is shown in Figure 7.

Unmodified alumina, six NaOH modified alumina samples, and five NaCl modified alumina samples were tested in this way. The

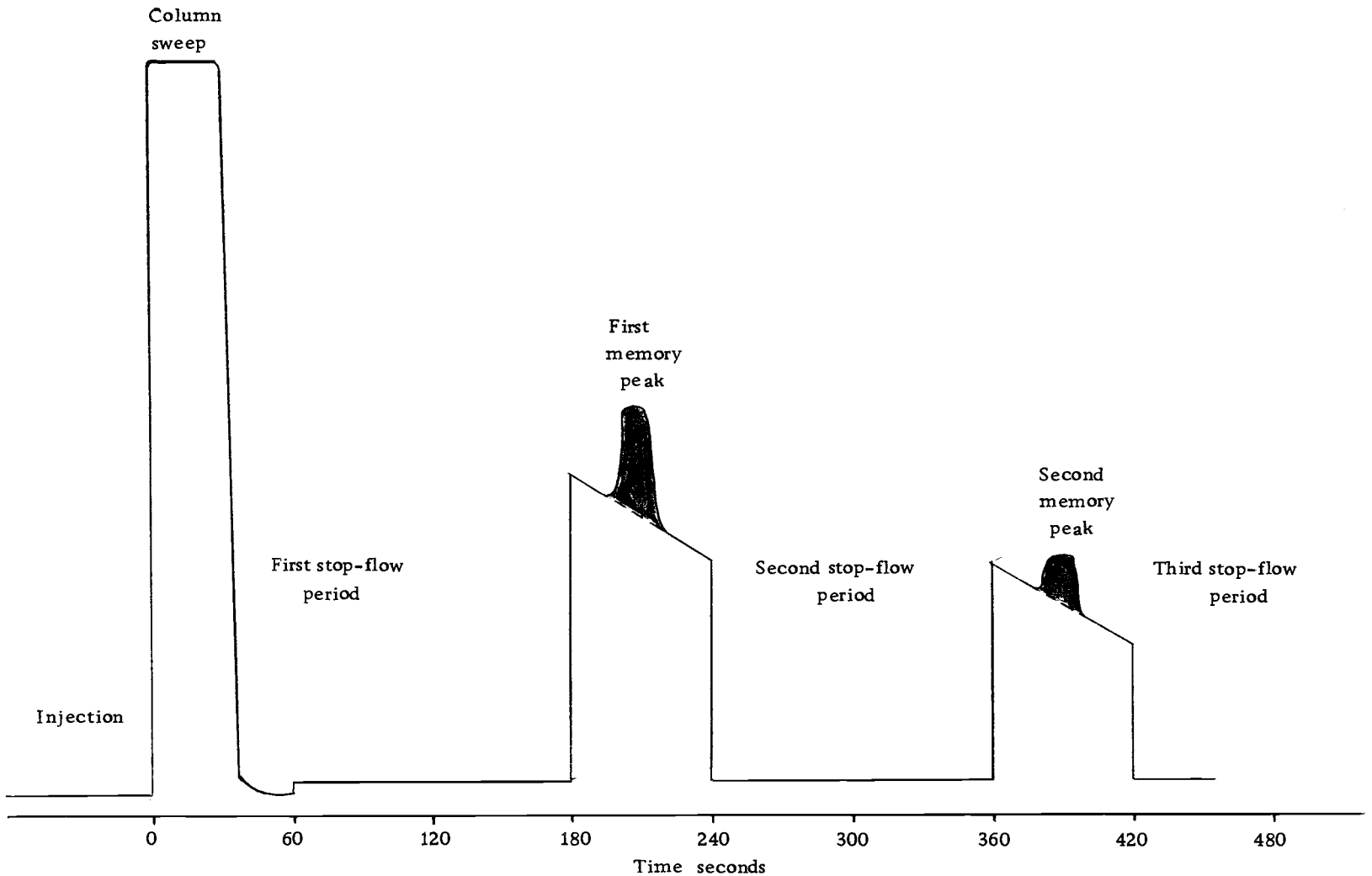


Figure 7. The output profile of the stopped-flow gas chromatograph. Shaded areas are memory peak areas.

NaOH surface modification ranged from 0.7 to 25 weight percent. The NaCl modified aluminas ranged from 0.6 to 5.8 weight percent. Each of these had their surface areas and pore diameters measured, as previously described.

The memory peak areas were measured by the Sternberg (32) method. The peak areas were expressed as fractions of the area produced by a known amount of methane injected after the column.

# IV. RESULTS AND DISCUSSION

## A. Modification of the Surface

The salt modification of the alumina surface as described by Scott (13) and Sawyer et al. (14) was first used, quantifying results with surface area measurements. The surface areas were expected to continually drop as the salt modification increased (7). The results were not good using this method as shown in Figure 8. The scatter of the points at modifications below 10% indicate problems with reproducibility and homogeneous surface coverages. The evaporation technique used by these researchers requires considerable time and stirring, causing fractionation of the particles. Allowing alumina to contact the salt solutions, especially NaOH, for several hours will not only cover the surface, but also react with it.

The procedure described in the experimental section was then utilized, as it is a method of coating stationary phases on supports in gas-liquid chromatography. It has the advantage of not having the salt solution in contact with the surface for long periods of time; the entire procedure takes about 30 minutes. The utilization of the vacuum pump to pull trapped air from the pores is necessary as a large volume of trapped air is removed when pumping begins as witnessed by the frothing of the solution. Most of the surface area is in pores of less than 1000 Å and all surface modifications must

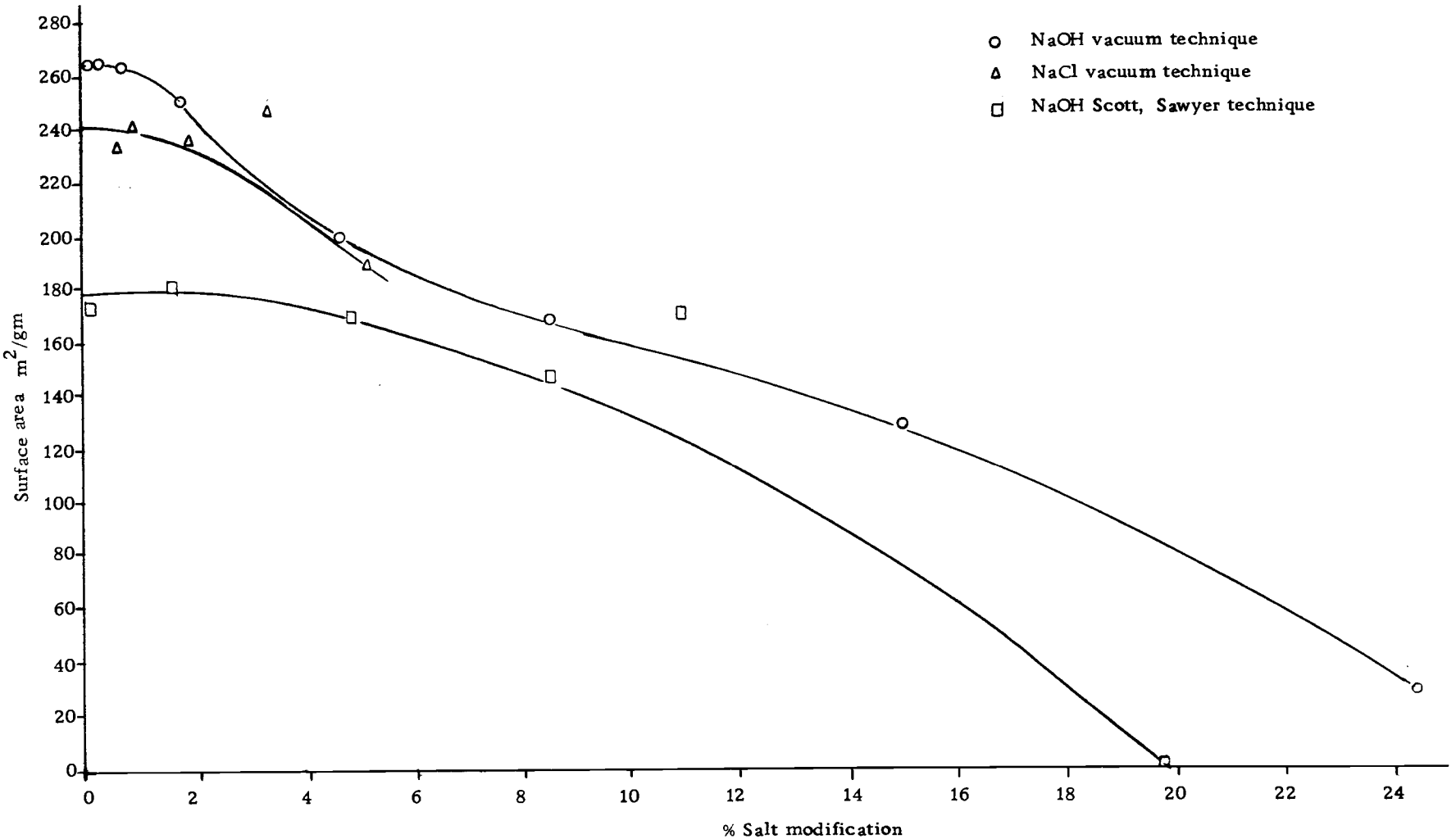


Figure 8. Effect of salt modification on adsorbent surface area.

have provisions to get the modifier inside of these pores.

The results of the modification procedure using the vacuum technique are encouraging. For NaOH, the surface area decreases gently as surface modification is increased as shown in Figure 8.

Sodium chloride modification proved to be quite different from NaOH modification (Table II). The volume of salt solution taken into the adsorbent pores decreased as NaCl concentration increased. This effect appears to be caused by the salt binding all the available water, increasing the surface tension of the water. When the NaCl modified surface areas were measured they compared well with the NaOH modified alumina, shown in Figure 8.

This data show that the maximum coverage for NaCl modified alumina is about 6%. In Table III, Brookman and Sawyer (14) found that some salts had very little effect on surface area at 10% weight/weight modification, while others changed the surface area considerably. This may be the same effect: actual surface coverage may be considerably smaller than 10%. The evaporate to dryness technique has no assurance the salt modifier is uniformly recrystallizing on the adsorbent surface.

## B. Pore Volumes

Most of the volume inside the particles were in pores less than 40 Å radius. The results were similar for all the samples as shown

Table II. Data from the NaOH and NaCl Modification of Alumina.

| Salt | Salt Sol. Conc. gm/100 ml | Volume of Soln. per 10 gm Adsorbent | % Modification Weight/Weight | BET Surface Area $m^2/gm$ |
|---|---|---|---|---|
| NaOH | 0.998 | 7.12 | 0.7 | 265 |
| NaOH | 2.080 | 8.25 | 1.8 | 252 |
| NaOH | 3.710 | 7.10 | 2.6 | 233 |
| NaOH | 10.020 | 8.53 | 8.5 | 170 |
| NaOH | 19.340 | 7.71 | 15.0 | 130 |
| NaOH | 28.150 | 6.96 | 24.0 | 28 |
| NaCl | 0.640 | 9.18 | 0.6 | 237 |
| NaCl | 0.900 | 8.56 | 0.8 | 240 |
| NaCl | 2.080 | 8.95 | 1.9 | 236 |
| NaCl | 5.870 | 5.84 | 3.4 | 250 |
| NaCl | 18.830 | 3.08 | 5.8 | 191 |

Table III. Effect of Salt Modification on Surface Area (14).

| | Area $m^2/gm$ |
|---|---|
| F-1 Alumina, acid wash (unmodified) (A) | 278 ± 7 |
| A + 10% NaCl | 269 ± 7 |
| A + 10% $Na_2SO_4$ | 254 ± 7 |
| A + 10% $Na_2M_0O_4$ | 279 ± 7 |
| A + 10% $Na_3PO_4$ | 210 ± 5 |
| A + 10% NaOH | 233 ± 6 |

in Figures 9-13. This, along with the decreasing surface areas for increased salt modification,indicate that the inner surfaces were modified and slightly changed. The pores were not plugged until 24% NaOH modification, where the surface area was very small and pores were nonexistent.

The NaOH modification eliminated most of the pores with radii between 20 and 40 Å. The NaCl, on the other hand, showed very few pores with radii less than 14 Å, with considerable sample being desorbed from pores with radii between 20 and 40 Å.

The pore volumes were not measured below 10 Å as several implied assumptions in the calculation are no longer valid. At this point, the pore radius is so small that the layers of molecules adsorbed on the surface significantly decrease the radius. There is no precise method to accurately estimate this number and the resultant error is very large.

## C. Development of the Stopped-flow Chromatograph

The initial design of this instrument came from a description by Phillips (5) of his stopped-flow chromatograph used for measuring reaction rates on catalysts. It had stopped-flow capabilities, a 1.8m column packed with adsorbent, and an injection port to introduce samples onto the column. With this design it was often difficult to discern where the memory peaks started and the previous peak tail

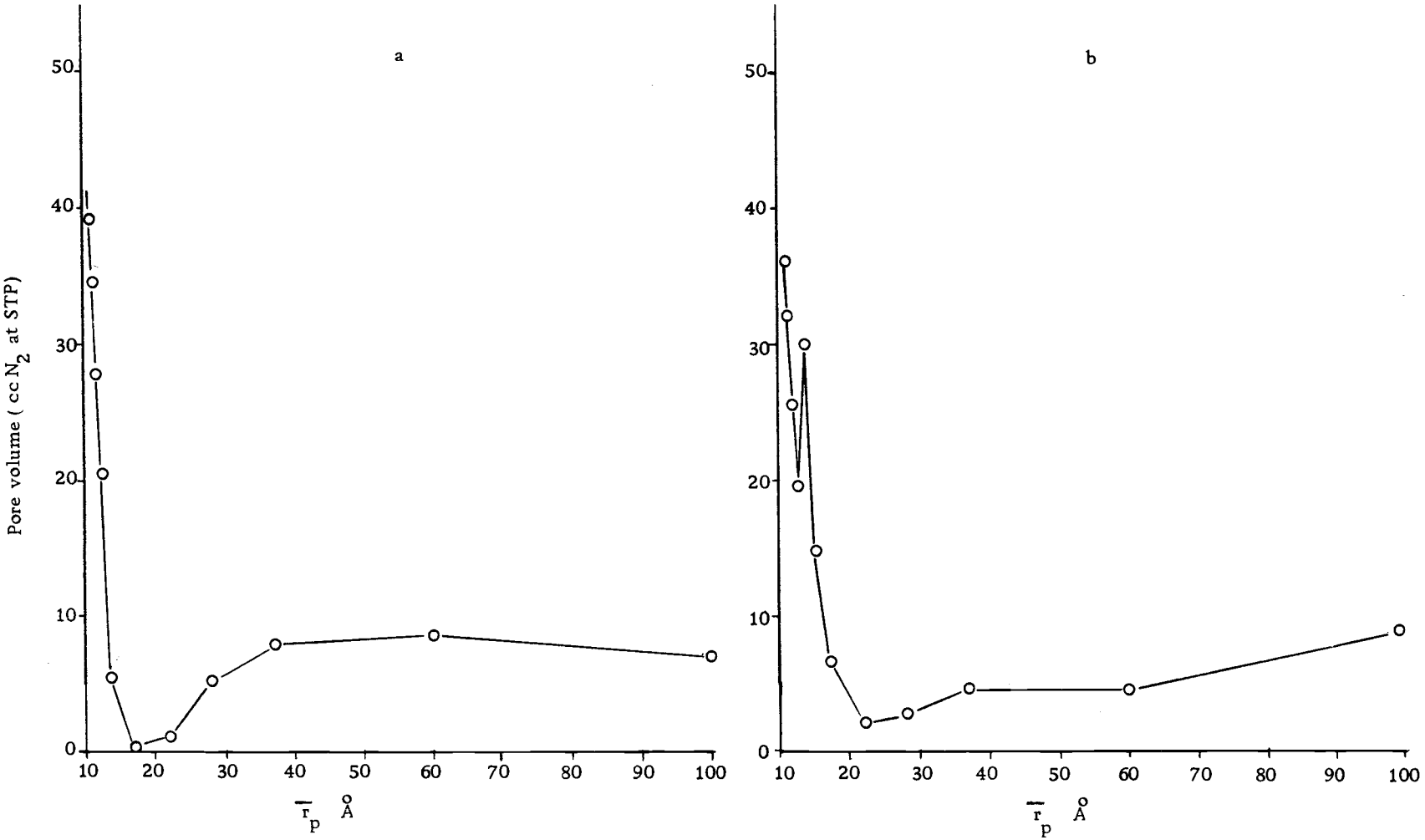


Figure 9. Pore volume distribution for a) unmodified alumina and b) 1.76% NaOH modified alumina.

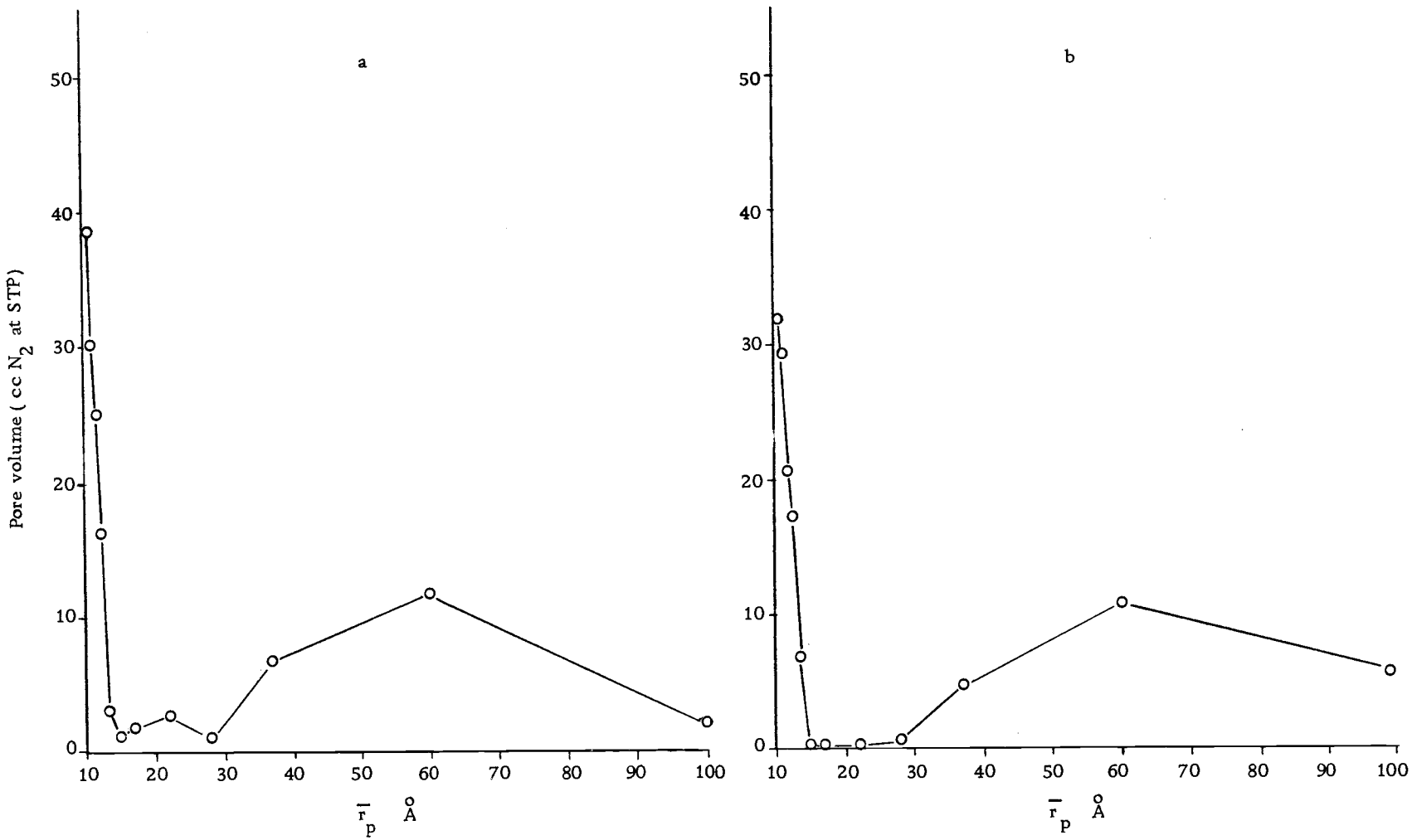


Figure 10. Pore volume distribution for a) 2.63% and b) 8.55% NaOH modified alumina.

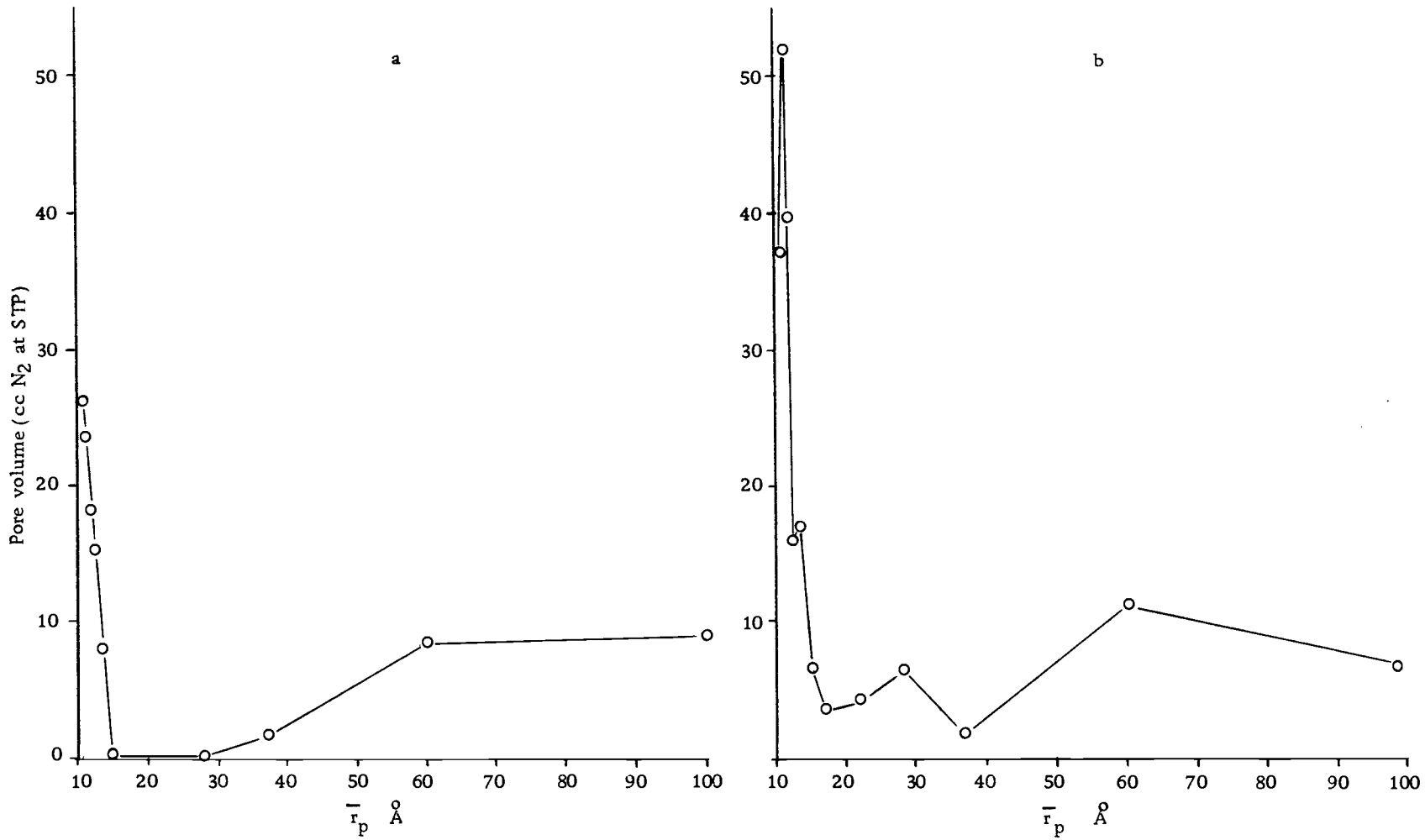


Figure 11. Pore volume distribution for a) 15% and b) 0.71% NaOH modified alumina.

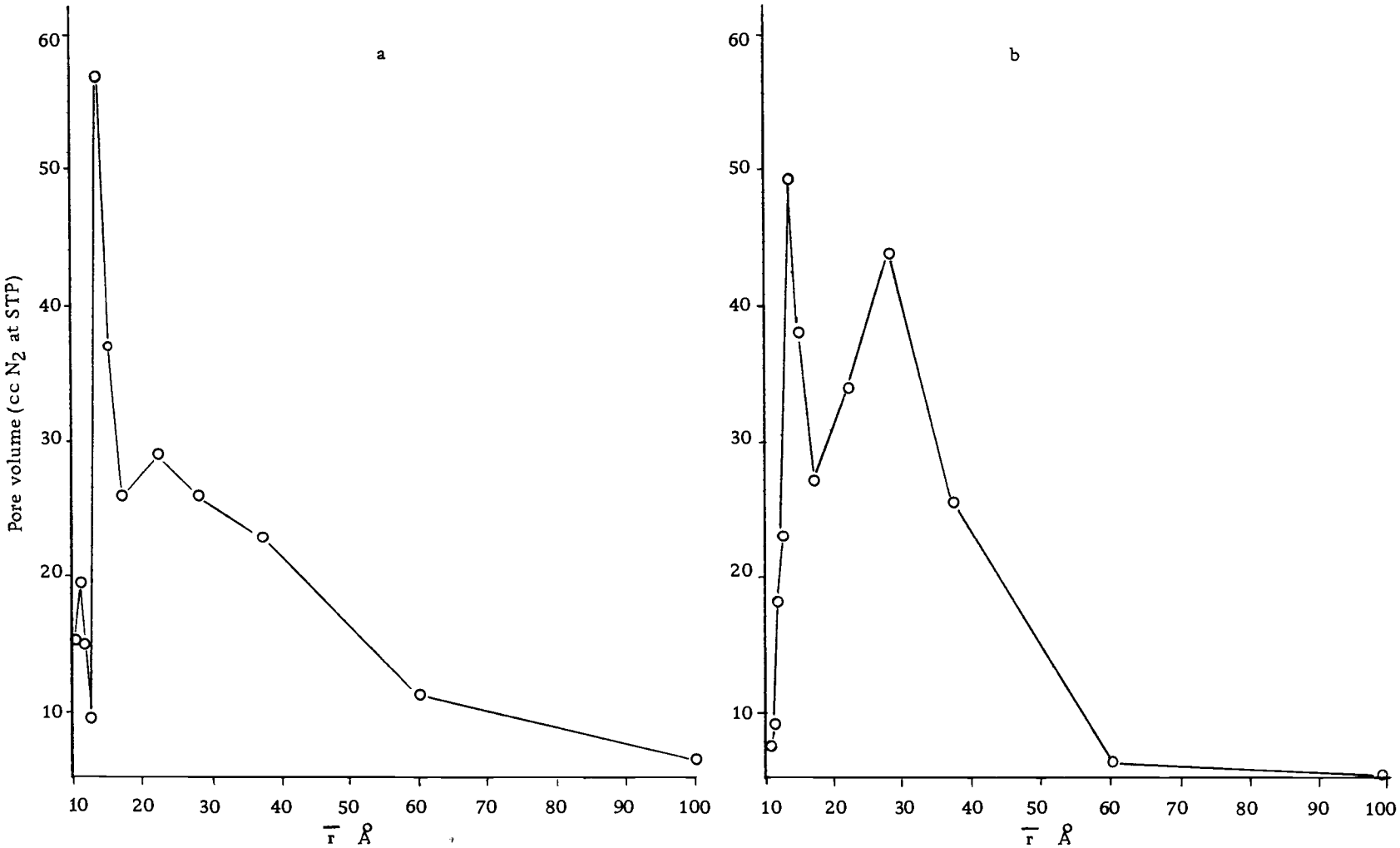


Figure 12. Pore volume distribution for a) 0.59% and b) 1.86% NaCl modified alumina.

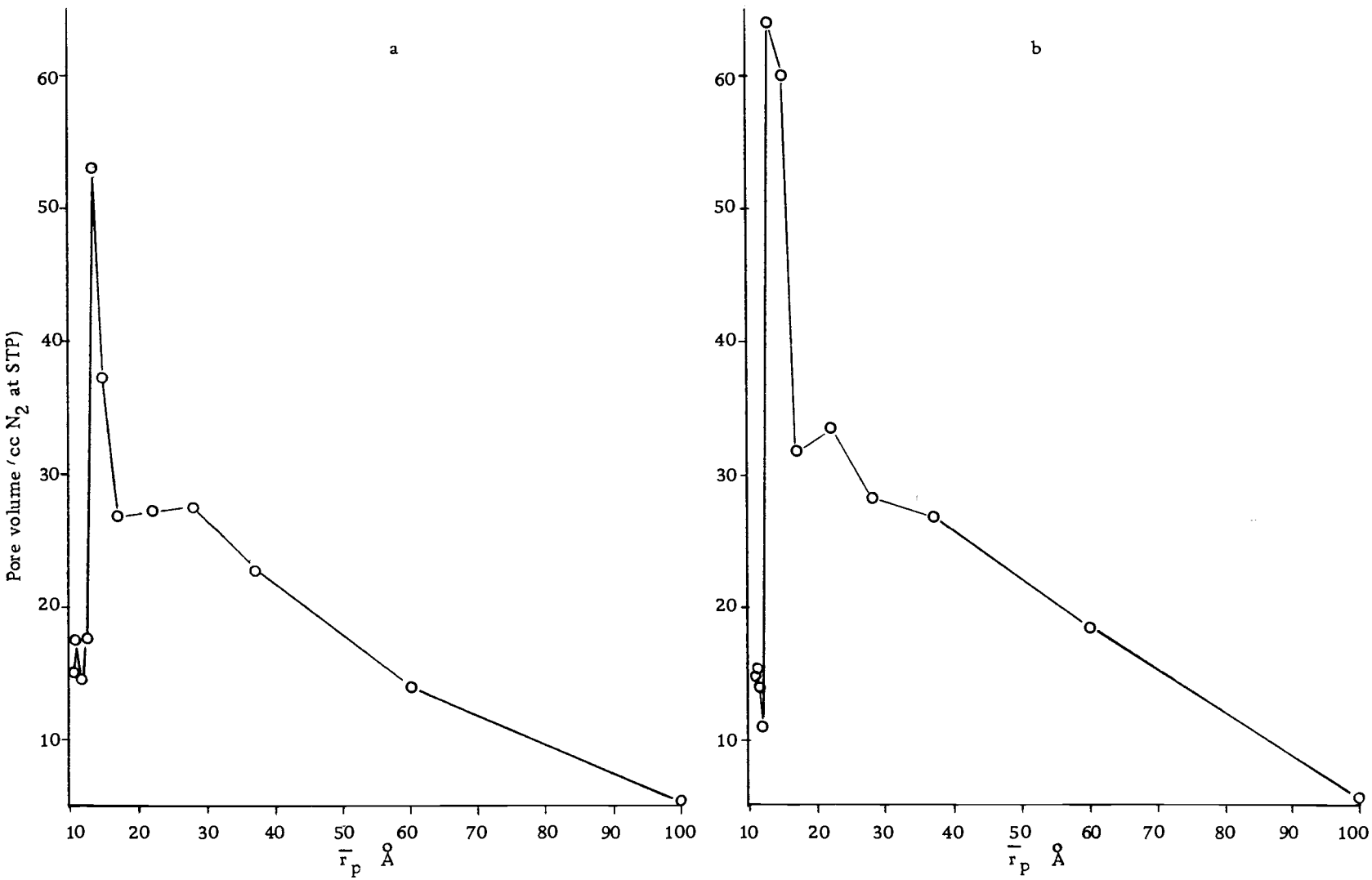


Figure 13. Pore volume distribution for a) 3.4% and b) 5.8% NaCl modified alumina.

ended. The stopped-flow-bypass valve caused its own memory peaks and the injection system had a large dead volume that collected and slowly released sample.

The second design had a 5 cm slug of adsorbent material instead of a long column. The inject-elute valve replaced the injection port and the gaseous sample was continually purged over the adsorbent for the desired injection period. This nearly eliminated the above problem of distinguishing material from the previous peak tail and the memory peak. Although this appeared to be better, other problems arose. Space in the oven was very short and leaks developed, especially around the adsorbent slug, causing memory peaks when there shouldn't have been any. The Viton 0-rings in the valves, with a maximum temperature of 200°C would not allow proper conditioning of the adsorbent surface. As temperature in the oven increased, the sensitivity of the detector decreased, making the higher temperatures considerably less sensitive than the lower temperatures as shown in Figure 14.

The third and final design is that described in the experimental section of this paper. The adsorbent slug was well separated from all valves and fittings by three feet of glass beads on each end of the column. Any trapped sample or anomolous flow patterns caused by these valves and connections could not interfere with the memory peaks of interest. The glass beads and the adsorbent slug were the

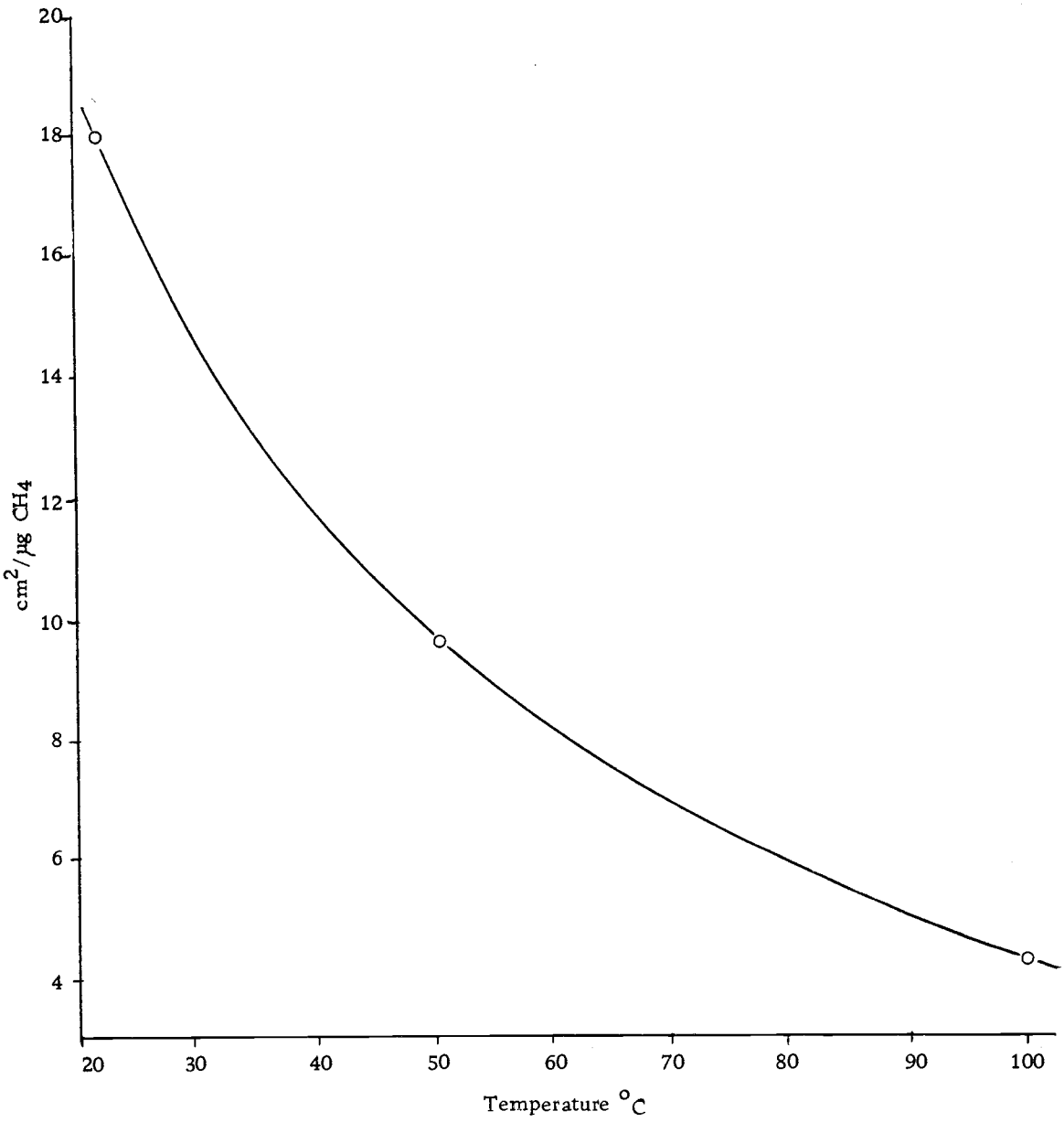


Figure 14. Sensitivity of the Carle thermoconductivity detector for 33 µg $CH_4$ at different temperatures.

only parts in the oven, allowing proper conditioning at 325°C for 24 hours. Outside the oven, the 0-rings in the valves lasted longer and leaked less, and the detector was at maximum sensitivity at all oven temperatures. Glass beads, No. 18, were packed in the tubes connecting the column outlet to the detector. Most of the pressure drop in the system, then, was across this part; i.e. there was negligible pressure drop across the column. This eliminated variations in flow with column packing technique, and changes in flow with changes in temperature of the oven. Since the column was isobaric, only minimum equilibration time was needed when the carrier flow was either started or stopped.

## D. Slow Process Measurement

The sample desorbed on the first memory peak after injection, are shown in Figures 15 and 16 for NaOH and NaCl modification of alumina respectively. In both cases, as the salt modification increased, and the surface area decreases, the size of the first memory peaks decreased, showing a lower initial amount of sample remaining for slow process release. The NaCl modified alumina memory peak decreased faster than the NaOH modified alumina.

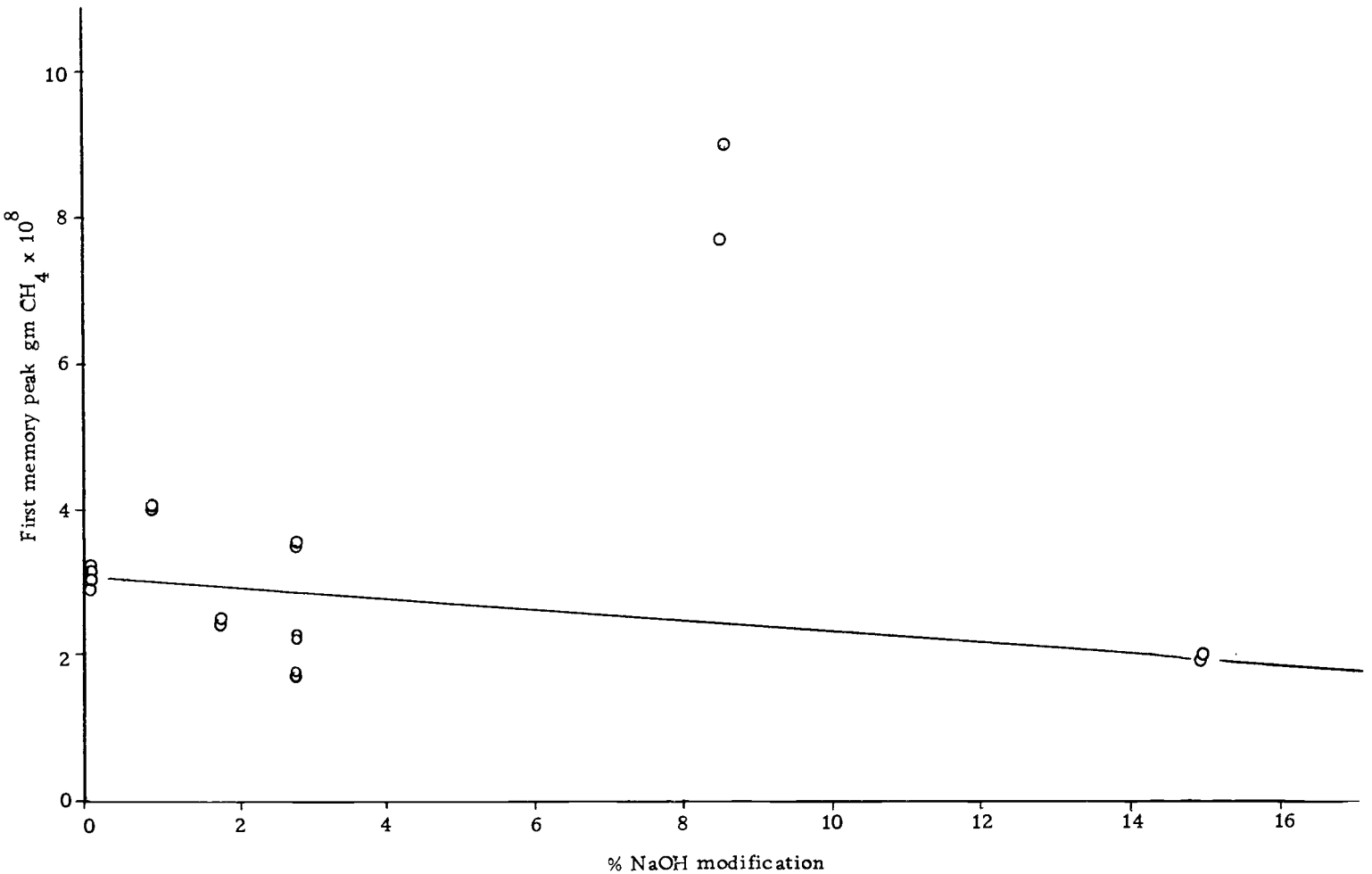


Figure 15. Mass of the first memory peak at various NaOH modifications.

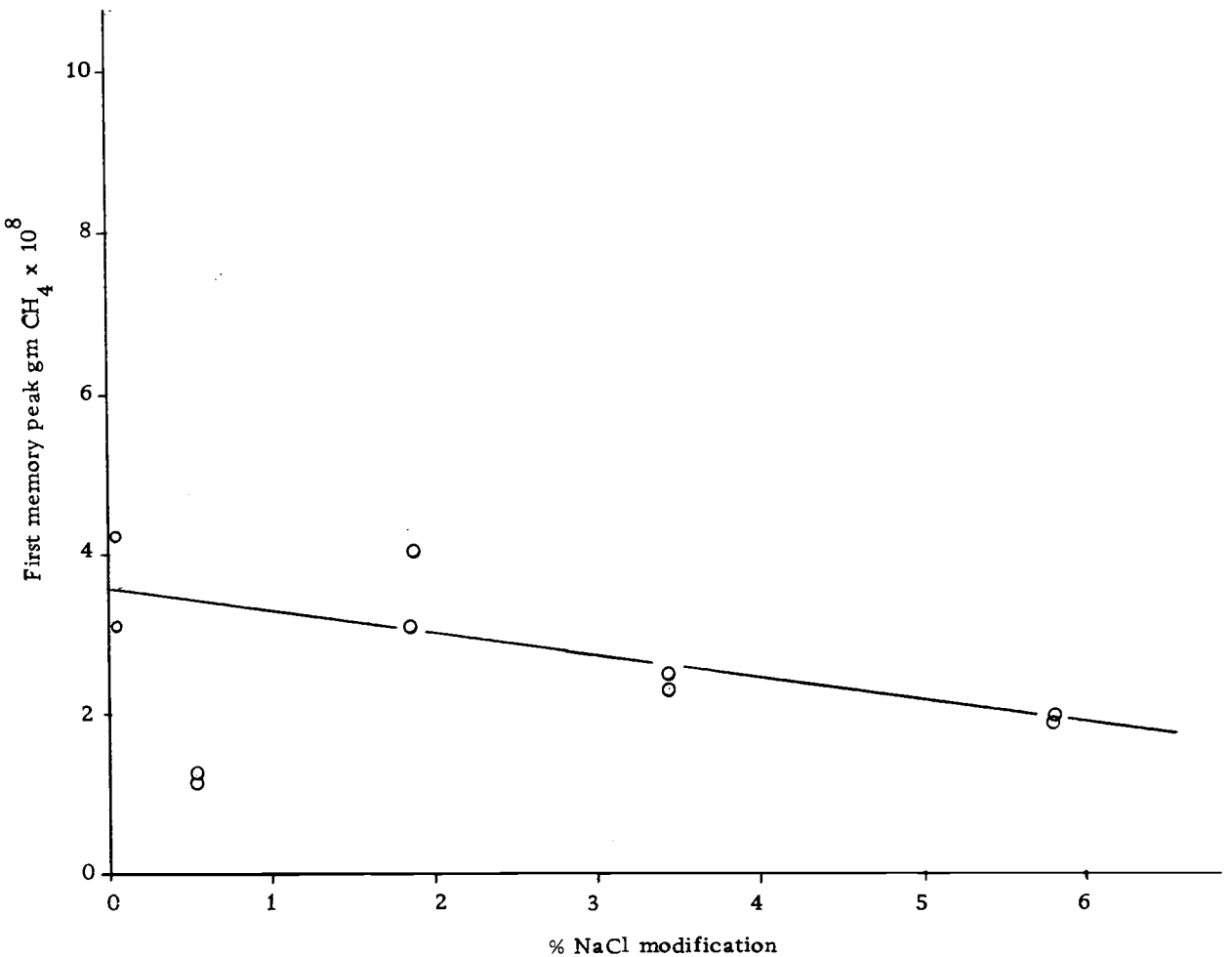


Figure 16. Mass of the first memory peak at various NaCl modifications.

## E. Slow Process Rate Constant

The slow process rate constant was determined by plotting the logarithm of sample mass versus total time, excluding the last stop-flow period as described by equation 22. Several of these are shown in Figure 17. Generally the curves are slightly concave, indicating higher order kinetics, measurement error of the smaller memory peaks, or two simultaneous reactions, one slightly faster than the other affecting the earlier memory peaks. Katsanos and Hadzistelios (18) found two rate constants when n-butane and trans-2-Butene were desorbed from 10% $CeCl_3$ modified $Al_2O_3$. The fastest process was 2 to 5 times faster than the slower process. This is believed to have occurred in this system as well, causing the first memory peak to be slightly larger than it should have been.

The slow process rate constant, k, was calculated using a linear least squares fit of the points and is plotted against percent salt modification, in Figure 18. A minimum rate constant is obtained at 0.71% NaOH modification and 1.9% NaCl modification. The NaOH rate constant again decreased at modification above 10%.

The reason for this slower reaction rate constant at less than 2% modification is not definite, but it appears the sample is diffusing from small pores. There are two reasons for this. First, no adsorption was expected for methane on alumina at 200°C. Second,

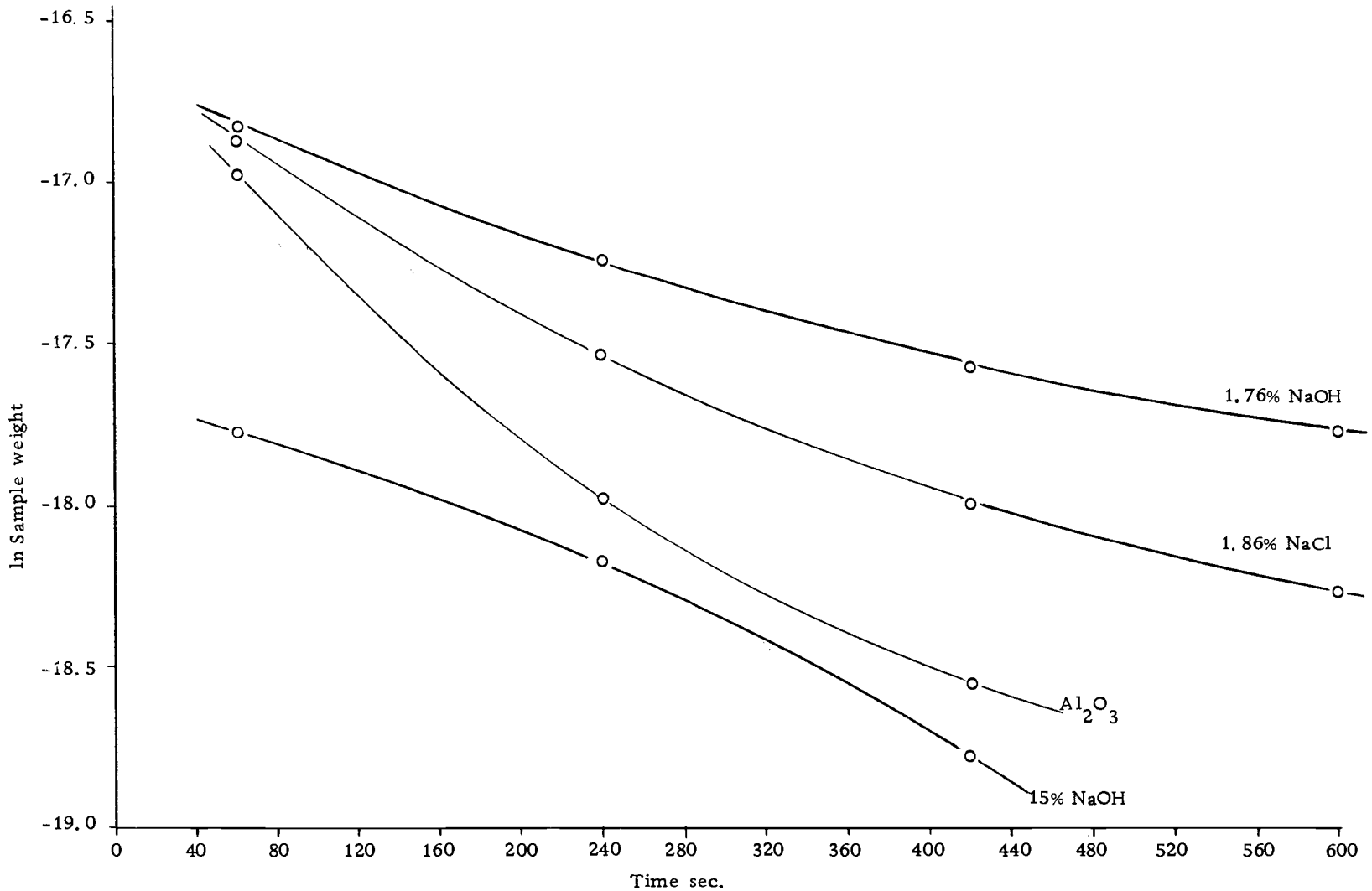


Figure 17. Log of successive memory peak mass versus time in the column. Slope gives rate constant k.

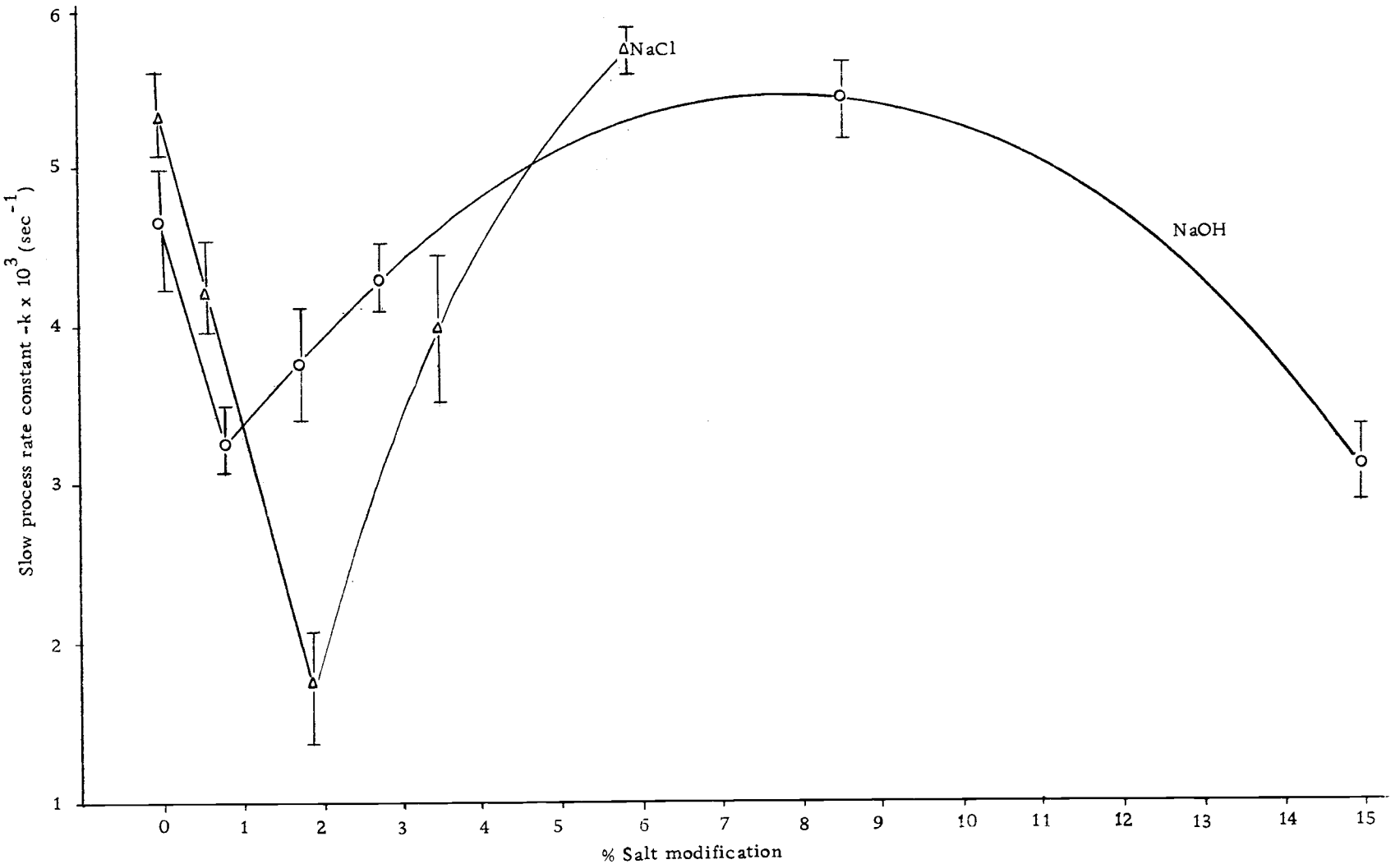


Figure 18. Rate constants k for the various salt modifications.

it would be expected that if the slow process measured was from desorption from active sites, then the unmodified alumina rate constant would be considerably lower and increasing rapidly as the active sites were covered by the salt modifier.

The pore volume distributions do not show any significant differences that would lead one to conclude the rates would be slower for the 0.71% NaOH and 1.9% NaCl. On the contrary, both of these samples have the lowest volumes of material in pores of 10 to 13 Å radius for their respective modification. This would lead to the opposite conclusion. However, if the pores during the modification process were reduced from 13 Å to about 5 Å by partially clogging the pore exit, then diffusion from the pore would be greatly reduced. At the NaOH modifications greater than 10% the same would be true.

When the rate constants shown in Figure 17, which had been obtained using methane at 200°C were compared to data collected by Katsanos and Hadzistelios (18) using n-butane from 60 to 100°C, the apparent activation energies[1] agreed very well as shown in Table IV. The logarithm of A (ln A), necessary in the Arrhenius equation, was obtained from their data and assumed to be 3.3 for this data.

The excellent comparison between our data and the "fastest"

---

[1]Molecules diffusing from pores do not have to cross an activation barrier. The term apparent activation energies is used to avoid confusion with chemical kinetic processes.

Table IV. Apparent activation energies for the slow process.

| | E(Kcal/mole) | log A |
|---|---|---|
| 10% $CeCl_3$[1] | 9.0[2] ± 0.1 | 2.3 |
| 10% $CeCl_3$[1] | 11.5[3] ± 0.01 | 3.3 |
| Alumina | 8.2 ± 0.2 | |
| Alumina | 8.0 ± 0.1 | |
| 0.7% NaOH | 8.5 ± 0.1 | |
| 1.8% NaOH | 8.4 ± 0.2 | |
| 2.6% NaOH | 8.2 ± 0.1 | |
| 8.5% NaOH | 8.0 ± 0.1 | |
| 15% NaOH | 8.5 ± 0.1 | |
| 0.6% NaCl | 8.2 ± 0.1 | |
| 1.9% NaCl | 9.0 ± 0.3 | |
| 3.4% NaCl | 8.3 ± 0.1 | |
| 5.8% NaCl | 8.0 ± 0.1 | |

[1] n-Butane as adsorbate (18).

[2] fastest slow process.

[3] slowest slow process.

slow process as measured by Katsanos et al. (18) indicate that the data originate from the same surface phenomenon. The relative harshness in which our data was collected ($CH_4$ as adsorbate, temperature at 200°C) would rule out the possibility of the methane being adsorbed on the surface. The methane must be diffusing from the very small pores. The "slowest" slow process for adsorption of n-butane at 100°C probably is an adsorption phenomenon from high energy adsorption sites.

# V. CONCLUSIONS

This thesis has shown that slow process causing chromatographic peak tailing on adsorbent particles, can result from at least one process; sample diffusion from pores less than 10 Å radius. The other process, desorption from high energy sites, was not monitored here. To decrease the diffusion from small pores, these pores must be either plugged, or filled during the manufacture or modification of the particles. This will significantly lower the surface area, and possibly the separating ability of the surface.

This thesis has also shown that the stopped-flow chromatograph can be a very useful tool to determine surface kinetic mehcanisms, diffusion kinetics in packed beds, and adsorption kinetics on adsorbent and catalytic surfaces.

# BIBLIOGRAPHY

1. Euken, A. and H. Knick, "Automatic Procedure for the Microanalytical Separation of Low Boiling Hydrocarbons by Desorption," Chem. Abstr., 31, 1727 (1937).

2. Ettre, L. S. and A. Zlatkis, "The Practice of Gas Chromatography," (Interscience, New York) 1967, p. 4.

3. James, A. T. and A. J. P. Martin, "Liquid-Gas Partition Chromatography," Biochem. J. (Proc.) 48 vii (1951).

4. Vernon, F., "Gas-Solid Chromatography on Modified Alumina Stationary Phase. I. Behavior of Aromatic Hydrocarbons," J. Chromatog. 60 (3) 406-410 (1971).

5. Cadogan, D. F. and D. T. Sawyer, "Gas Chromatographic Studies of Surface Complexes formed by Aromatic Molecules with Lanthanum Chloride on Silica Gel and Graphon," Anal. Chem. 43 (7) 941-943 (1971).

6. Giddings, J. C., "Dynamics of Chromatography," (Dekker, New York) 1965, pp. 255-262.

7. Phillips, C. S. G. and C. G. Scott, "Modified Solids for Gas-Solid Chromatography," Advances in Analytical Chemistry and Instrumentation, Vol. 6, J. H. Purnell, ed. (Interscience, New York) 1968, pp. 121-152.

8. Oberholtzer, J. E. and L. B. Rogers, "Effects of Micropores on Peak Shape and Retention Volume in Gas-Solid Chromatography," Anal. Chem. 41 (12) 1590-1594 (1969).

9. Habgood, H. W. and J. F. Hanlan, "A Gas Chromatographic Study of the Adsorptive Properties of a Series of Activated Charcoals," Can. J. Chem. 37, 843, (1959).

10. DiCorcia, A., D. Fritz, and F. Bruner, "Use of Graphitised Carbon Black for Linear Gas-Liquid-Solid Chromatography of Polar Low Boiling Compounds," Anal. Chem. 42 (13) 1500-1504 (1970).

11. Dandeneau, R. D. and S. J. Hawkes, "Fast Gas Chromatography," To be published (Academic Press) 1977.

12. Hargrove, G. L. and D. T. Sawyer, "Thermodynamics and Separation Efficiencies for Gas-Solid Chromatography with Modified Alumina Columns," Anal. Chem. 40 (2) 409-413 (1968).

13. Scott, C. G., "Linear Gas-Solid Chromatography," Gas Chromatography, 1962. M. vanSwaay. ed. (Butterworths, London) 1963, pp. 36-62.

14. Brookman, D. J. and D. T. Sawyer, "Specific Interactions Affecting Gas Chromatographic Retention for Modified Alumina Columns," Anal. Chem. 40 (1) 106-110, (1968).

15. Gerber, J. N. and D. T. Sawyer, "Nature of Nonspecific Interactions in Gas-Solid Chromatography," Anal. Chem. 44 (7) 1199-1203 (1972).

16. Kiselev, A. V. and Y. I. Yashin, "Gas Adsorption Chromatography," (Plenum Press, New York) 1969.

17. Phillips, C. S. G., M. J. Walker, C. R. McIlwrick, and P. A. Rasser, "Slow Processes and Gas Chromatography," J. Chromatog. Sci. 8, 401-404 (1970).

18. Katsanos, N. A. and I. Hadzistelios, "Kinetic Study of Slow Processes in Gas Chromatography," J. Chromatog. 105 (1) 13-23 (1975).

19. Schupp, O. E., "Gas Chromatography in Techniques of Organic Chemistry," Vol. XIII, (Interscience, New York) 1968, p. 52.

20. Dacey, J. R., "Active Carbon," in The Solid-Gas Interface, E. A. Flood, ed., (Marcel Dekker, New York) 1967, Vol. 2, pp. 995-1024.

21. Giddings, J. C., "Dynamics of Chromatography," (Dekker, New York) 1965, pp. 95-118.

22. Giddings, J. C., "Dynamics of Chromatography," (Dekker, New York) 1965, p. 262.

23. Linsen, B. G. and A. van den Heuvel, "Pore Structures," in The Solid-Gas Interface, E. A. Flood, ed., (Marcel Dekker, New York) 1967, Vol. 2, p. 1027.

24. Barrer, R. M., "Surface and Volume Flow in Porous Media," in The Solid-Gas Interface, E. A. Flood, ed., (Marcel Dekker, New York) 1967, Vol. 2, p. 573.

25. Linsen, B. G. and A. van den Heuvel, "Pore Structures" in The Solid-Gas Interface, E. A. Flood, ed., (Marcel Dekker, New York) 1967, Vol. 2, pp. 1046-1047.

26. Barrer, R. M., "Surface and Volume Flow in Porous Media," in The Solid-Gas Interface, E. A. Flood, ed., (Marcel Dekker, New York) 1967, Vol. 2, p. 581.

27. Giddings, J. C., "Dynamics of Chromatography," (Dekker, New York) 1965, pp. 191-192.

28. Moore, W. J., "Physical Chemistry," (Prentice Hall, New Jersey) 1972, p. 363.

29. Laidler, K. J., "Chemical Kinetics," (McGraw-Hill, New York) 1965, pp. 14-15.

30. Slabaugh, W. H. and A. D. Stump, "Surface Areas from the V/n Ratio for Marine Sediments," J. Phys. Chem., 68 (5), pp. 1251-1253 (1964).

31. Pierce, C., "Computation of Pore Size from Physical Adsorption Data," J. Phys. Chem., 57, pp. 149-152 (1953).

32. Sternberg, J. C., "Extra column Contributions to Chromatographic Band Broadening," in Advances in Chromatography, J. C. Giddings and R. A. Keller, ed., (Marcel Dekker, New York) 1966, Vol. 2, p. 214.

# APPENDIX

# APPENDIX I

## CALCULATION OF PORE VOLUME DISTRIBUTION

Terms used:

$P/P_0$ - the partial pressure at the particular point being analyzed (from the isotherm).

Mg $N_2$/gm - the weight of adsorbed $N_2$ per gm adsorbent (read off isotherm).

$V_{cc}$ - volume of the adsorbed $N_2$/gm adsorbent at STP.

$\Delta V$ - the difference in $V_{cc}$ between the $n^{th}$ and n + 1 reading and is the total volume being desorbed.

n - the number of adsorbed layers of adsorbate for each $P/P_0$.

$\Delta n$ - the change in number of adsorbed layers between the nth and n + 1 reading.

$\Delta V_f$ - a correction term, after the first desorption increment, for gas desorbed from the wall film of previously empty pores.

$\Delta V_k$ - the volume from the pores being emptied.

R - the ratio $(r_p)^2/(r_k)^2$.

$V_p$ - the gas volume of $N_2$ at STP in the pore radius $r_p$.

$r_p$ - the pore radius and is larger than $r_k$ by the adsorbed film thickness.

$\bar{r}_p$ - the average pore radius between reading n and (n + 1).

$A_p$ - the pore surface area in $m^2$ for the average pore radius of interest.

To begin, the easiest method is to set a table as in Table V. Specified $P/P_0$ values are used to obtain good results. If the

desorption branch has the greatest change in the slope at $P/P_0 \leq 0.40$, then the most samples should be taken in that area. Figure 19 is then used to obtain n, R, and $r_p$ for each $P/P_0$. Delta n ($\Delta n$) and $\bar{r}_p$ are then calculated by taking the difference and the average of the $n^{th}$ and n + 1 values respectively. The (mg $N_2$/gm) reading is obtained from the desorption branch of the isotherm. $V_{cc}$ is calculated by

$$V_{cc} = \frac{(\text{mg } N_2/\text{gm})\,(22.4 \text{ l/mole})}{28 \text{ gm/mole}} \qquad \text{Eq. 27}$$

and represents the volume of gas at STP that is adsorbed onto the surface. The $\Delta V$ column can then be calculated by subtracting the $V_{cc}$ value at the n + 1 reading from the $V_{cc}$ at the $n^{th}$ reading.

From this point on, each row must be calculated before the next row can be completed, because the wall film thickness correction $\Delta V_f$ is calculated by

$$\Delta V_f = (\Sigma A_p) \times (\Delta n) \times (0.23) \qquad \text{Eq. 28}$$

where the constant 0.23 is the gas volume of $N_2$ to form a single layer on one square meter of surface. The first row will have no correction factor so $\Delta V_f = 0$. The volume of the capillaries emptied $V_k$, over the selected $P/P_0$ range is obtained by

$$\Delta V_k = \Delta V - \Delta V_f \qquad \text{Eq. 29}$$

The total volume in the pores $V_p$ is related to the volume of $N_2$ that came out of the capillary by

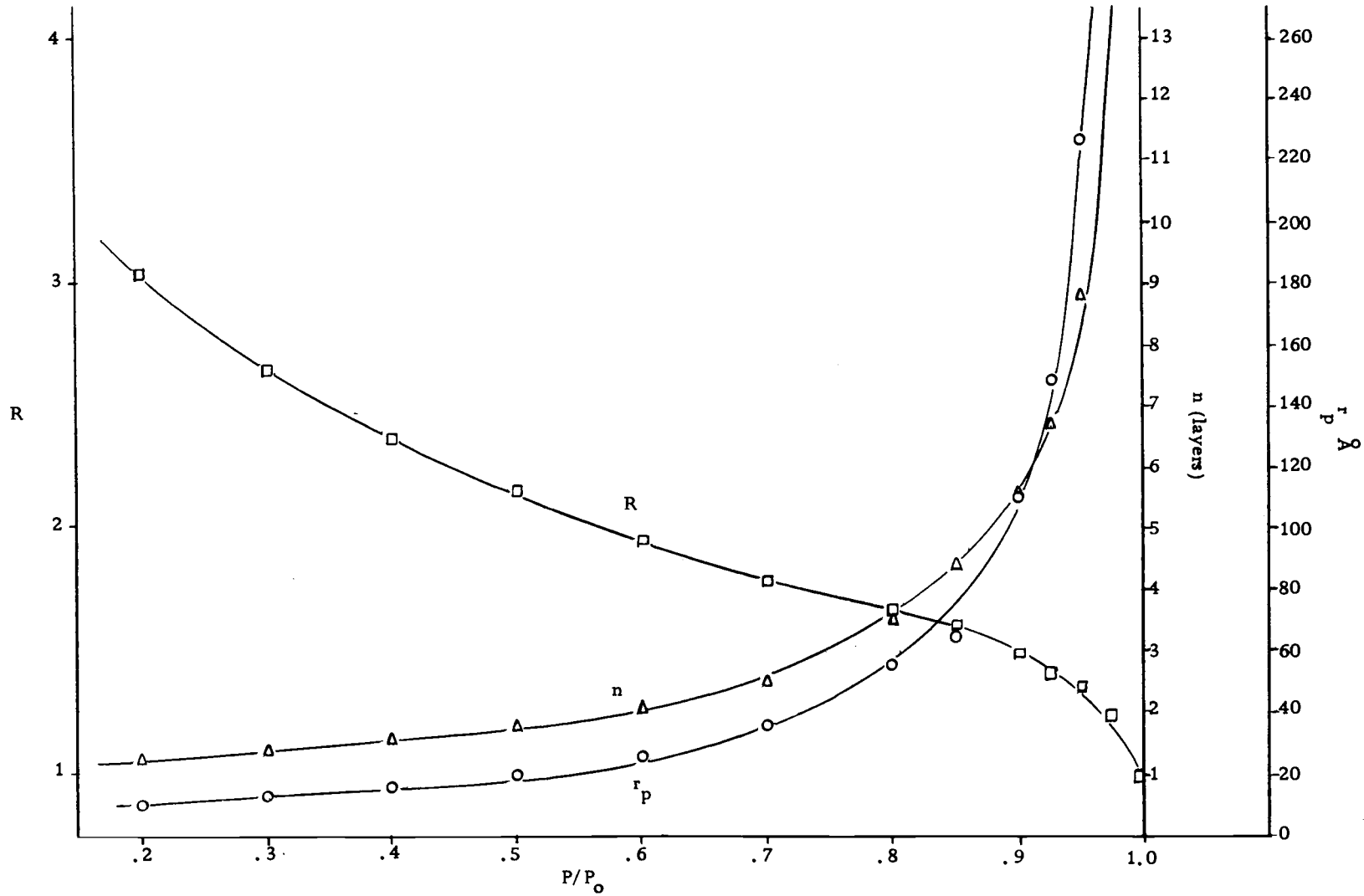


Figure 19. Values of n, R, and $r_p$ at various P/P$_o$ of $N_2$ to calculate pore volume distributions (31).

$$V_p = R\, V_k \qquad \text{Eq. 30}$$

where

$$R = (r_p)^2/(r_k)^2 \qquad \text{Eq. 31}$$

The pore radius $r_p$ is larger than the capillary radius $r_k$ by the wall film thickness of the adsorbed $N_2$.

The pore area $A_p$ in $m^2$ is given by

$$A_p = \frac{31\, V_p}{\bar{r}_p} \qquad \text{Eq. 32}$$

and a running total, $\Sigma A_p$, is maintained in the last column for calculation of $\Delta V_f$ in the next row.

The pore volume $V_p$ for each average pore radius $\bar{r}_p$ produce the histograms shown in the text, Figures 9-13.

Table V. Calculation of pore volume distribution.

| $P/P_0$ | $\frac{mg\ N_2}{gm}$ | $V_{cc}$ | $\Delta V$ | n | $\Delta n$ | $\Delta V_f$ | $\Delta V_k$ | R | $V_p$ | $r_p$ | $\bar{r}_p$ | $A_p$ | $\Sigma A_p$ |
|---|---|---|---|---|---|---|---|---|---|---|---|---|---|
| .900 | 332 | 265.6 | | 19.00 | | | | | | 120.0 | | | |
| .850 | 327 | 261.6 | 4.0 | 4.40 | 14.60 | 0 | 4.00 | 1.60 | 6.40 | 75.0 | 100.00 | 1.32 | 1.32 |
| .750 | 317 | 253.6 | 8.0 | 2.90 | 1.50 | 0.455 | 7.54 | 1.70 | 12.83 | 44.0 | 60.00 | 6.62 | 7.95 |
| .650 | 300 | 240.0 | 13.6 | 2.22 | 0.68 | 1.240 | 12.36 | 1.86 | 22.89 | 30.0 | 37.00 | 19.25 | 27.20 |
| .550 | 281 | 224.8 | 15.2 | 1.87 | 0.35 | 2.190 | 13.01 | 2.00 | 26.02 | 26.0 | 28.00 | 28.81 | 56.01 |
| .450 | 261 | 208.8 | 16.0 | 1.63 | 0.24 | 3.090 | 12.91 | 2.26 | 29.17 | 18.0 | 22.00 | 41.10 | 97.11 |
| .400 | 244 | 195.2 | 13.6 | 1.53 | 0.10 | 2.230 | 11.37 | 2.36 | 26.82 | 16.0 | 17.00 | 48.92 | 146.02 |
| .350 | 222 | 177.6 | 17.6 | 1.45 | 0.08 | 2.690 | 14.91 | 2.49 | 37.13 | 14.0 | 15.00 | 76.74 | 222.80 |
| .300 | 190 | 152.0 | 25.6 | 1.37 | 0.08 | 4.090 | 21.50 | 2.66 | 57.19 | 13.0 | 13.50 | 131.33 | 354.10 |
| .275 | 178 | 142.4 | 9.6 | 1.30 | 0.07 | 5.700 | 3.90 | 2.74 | 9.63 | 12.0 | 12.50 | 23.90 | 378.00 |
| .250 | 166 | 132.8 | 9.6 | 1.25 | 0.05 | 4.350 | 5.25 | 2.84 | 14.91 | 11.5 | 11.75 | 39.40 | 417.00 |
| .225 | 154 | 123.2 | 9.6 | 1.22 | 0.03 | 2.870 | 6.72 | 2.95 | 19.82 | 11.0 | 11.25 | 54.62 | 472.00 |
| .200 | 145 | 116.0 | 7.2 | 1.20 | 0.02 | 2.160 | 5.03 | 3.06 | 15.39 | 10.5 | 10.75 | 44.39 | 516.00 |